JAERI-Research
99-014

AC LOSS CALCULATION OF CENTRAL SOLENOID MODEL COIL

March 1999

Attila GILANYI*, Masato AKIBA, Yoshikazu OKUMURA,
Makoto SUGIMOTO, Yoshikazu TAKAHASHI and
Hiroshi TSUJI

日本原子力研究所
Japan Atomic Energy Research Institute

本レポートは、日本原子力研究所が不定期に公刊している研究報告書です。
入手の問合わせは、日本原子力研究所研究情報部研究情報課（〒319-1195　茨城県那珂郡東海村）あて、お申し越しください。なお、このほかに財団法人原子力弘済会資料センター（〒319-1195　茨城県那珂郡東海村日本原子力研究所内）で複写による実費領布を行っております。

This report is issued irregularly.
Inquiries about availability of the reports should be addressed to Research Information Division, Department of Intellectual Resources, Japan Atomic Energy Research Institute, Tokai-mura, Naka-gun, Ibaraki-ken 319-1195, Japan.

編集兼発行　日本原子力研究所

AC Loss Calculation of Central Solenoid Model Coil

Attila GILANYI*,Masato AKIBA, Yoshikazu OKUMURA,
Makoto SUGIMOTO, Yoshikazu TAKAHASHI and Hiroshi TSUJI

Department of Fusion Engineering Research
Naka Fusion Research Establishment
Japan Atomic Energy Research Institute
Naka-machi, Naka-gun, Ibaraki-ken

(Received January 28, 1999)

The AC loss of Central Solenoid Model Coil of ITER is calculated in order to be able to determine the allowable excitation current shape in time with respect to the available cooling capacity at liquid helium temperature.

In Part A the theory is summarized essential to present calculation. This covers a semianalytical integral formulation to calculate the magnetic field distribution in the cross-section of a coil and also 2D and 3D differential formulations for eddy current calculation of jackets and structural steel components, respectively.

In Part B the conditions and results of calculation are described in detail. Losses are calculated separately in different components. Also the different types of losses are separated, and only one of the followings is considered in the same time; eddy current loss, ferromagnetic hysteresis loss, superconducting hysteresis loss, coupling loss.

The low frequency eddy current loss calculations of structural stainless steel components are carried out by ANSYS/EMAG code in 3D separately for tension rods, plates and beams. The problem of loop currents is briefly discussed, but the interaction between several components is not considered.

In the case of Incoloy jackets of conductors a 2D ANSYS code is used with current force to obtain the eddy current losses. The ferromagnetic hysteresis

* Technical University of Budapest

loss of jackets are also roughly estimated based on measurement data.

The superconducting hysteresis and coupling losses of Nb_3Sn strands are estimated using measurement data and a calculated flux density distribution in the cross-section of the model coil by a semi-analytical integral formulation. The coupling is not considered during hysteresis loss calculation and an ideal model is used for coupling loss calculation.

The losses of Butt-type and Lap-typejoints and roughly estimated based on measurement data to make complete this study. Both the loss due to flux change and the loss due to transport current are considered.

The individual loss components are summed up, compared and plotted in time. The followings are concluded. The coupling loss was found to be the largest 83% of the total AC loss supposing 50 msec characteristic time constant. Also significant amount of heat is generated in structural steels, the largest amount in lower tension plates and inner tension rods. Therefore cooling is required for stainless steel structural components. The loss of joints is not large, however concentrated, therefore joints should receive attention. Specially Lap-type joints are critical components.

The eddy current and coupling power losses can be significantly decreased by increasing the ramp-up time since they are proportional to the square of flux change rate, while superconducting and ferromagnetic hysteresis power losses decrease linearly with decreasing flux change rate. Joule losses are produced in joints even after the energizing process of the magnet, when it is driven by a constant excitation current. This propose us to keep the time of full power operation short.

Keywords: CS Model Coil, AC Loss, Heat Generation, FEM, Eddy Current

CSモデル・コイルの交流損失解析

日本原子力研究所那珂研究所核融合工学部
Attila GILANYI*・秋場 真人・奥村 義和
杉本 誠・高橋 良和・辻 博史

（1999年1月28日受理）

ITER-CSモデル・コイルの交流損失を、試験整備の冷却能力から許容できる励時速度を把握するため解析した。

前編Aでは、ジャケット及び支持構造材に発生する渦電流を2次元及び3次元にて解析的に求めるための理論をまとめた。

後編Bでは、CSモデル・コイルの具体的な交流損失の発生量をまとめた。CSモデル・コイルに発生する渦電流損失、ヒステリシス損失、結合損失をそれぞれ個別に求めた。

支持構造物に発生する渦電流損失は汎用有限要素法コードANSYSを用いて解析した。また、導体ジャケット部の渦電流損失もANSYSを用いて解析した。導体ジャケット部のヒステリシス損失は実験データから求めた。超電導素線のヒステリシス損部（ジョイント部）に発生する交流損失を求めた。

解析の結果、CS モデル・コイルに発生する結合損失の割合が最も大きく、最大で全交流損失の83%を占める。また渦電流損失による発熱量は、支持構造物から発生するものが支配的である。特に下部テンション・プレートと呼ばれる構造物からの発熱が大きい。

那珂研究所：〒311-0193 茨城県那珂郡那珂町向山801-1
＊ ブタペスト工科大学

This is a blank page.

Contents

目　　次

Part A
Overview of Theory

This is a blank page.

1. Introduction

In Part A the theory essential to the loss calculation of CS Model Coil is summarized.

In Section 2 integral approaches are reviewed. First a formula is given to determine the magnetic field in the axis of a circular current carrying loop. Next the field distribution is determined in the axis of a thin solenoid. This is followed by a semi-analytical method using elliptic integrals applicable to the calculation of flux density distribution in the cross-section of a current carrying circular loop. Formulations for magnetic materials are also briefly discussed.

In Subsection 2.6 a simple formulation is introduced for low-frequency eddy current loss calculation of a conductive rod placed parallel to the magnetic field. The importance of this simple test case is to understand the frequency and specific resistivity dependence of power loss.

In Section 3 the 3D differential formulation is discussed for the eddy current loss calculation of tension rods, beams and plates.

In Section 4 some remarks are done for 2D eddy current calculations with differential formulation. The current force is introduced in order to make possible the 2D simulation of eddy currents in Incoloy jackets. To avoid problems with singularities in cylindrical coordinate system, two possible methods are briefly summarized.

The AC loss of superconducting cables is reviewed in the last section. The focus is on the hysteresis properties of superconductors and on the coupling, because these phenomena produce the main part of the loss.

2. Integral Approach

The magnetic field of quasi stationer currents can be described by the following set of Maxwell's equations

$rot\, H = J$,

$div\, B = 0$,

$B = \mu_0 H$.

Introducing the magnetic vector potential as $B = rot\, A$, we obtain

$rot\, rot\, A = grad\, div\, A - \Delta A = \mu_0 J$.

Selecting the divergence of A to be zero

$\Delta A = -\mu_0 J$

The solution for the magnetic vector potential can be obtained in the form of

$$A = -\frac{1}{4\pi}\int_V \frac{\Delta A}{r} dV + \frac{1}{4\pi}\oint_S \frac{\partial A}{\partial n}\frac{1}{r} dS - \frac{1}{4\pi}\oint_S A \frac{\partial}{\partial n}\frac{1}{r} dS$$

where S denotes the surface of volume V. If the components of A disappear enough far in the infinity , we can write

$$\bar{A} = \frac{\mu_0}{4\pi}\int_V \frac{\bar{J}}{r} dV \qquad \text{Eq. 2.1}$$

From now on the vectors will be notified with upper bars till the end of this section. For a current carrying circular loop introducing $\bar{J}dV = \bar{J}S\bar{dl} = I\bar{dl}$ we obtain

$$\bar{A} = \frac{\mu_0 I}{4\pi}\oint_l \frac{\bar{dl}}{r} \qquad \text{Eq. 2.2}$$

In a given point P the flux density is

$$\bar{B}(P) = rot_P \bar{A} = \frac{\mu_0 I}{4\pi} rot_P \oint_l \frac{\bar{dl}}{r}$$

Using the identity

$rot(\bar{u}\bar{v}) = u\, rot\, \bar{v} + grad\, u \times \bar{v}$

and substituting $u = \frac{1}{r}$ and $\bar{v} = \bar{dl}$

$$rot\frac{\bar{dl}}{r} = \frac{1}{r} rot\, \bar{dl} + grad\frac{1}{r} \times \bar{dl} = -\frac{\bar{r}}{r^3} \times \bar{dl}$$

because $rot_P \bar{dl} = 0$. By this we obtain the well-known Biot-Savart law

$$\bar{H} = \frac{I}{4\pi}\oint_l \frac{\bar{dl} \times \bar{r}}{r^3} \qquad \text{Eq. 2.3}$$

which allows us to evaluate the magnetic field generated by a current carrying conductor with arbitrary shape. This is the starting point of many analytical and semi analytical formulations.

2.1 Current Carrying Circular loop

First let us consider a circular loop with radius R and carrying current I as shown in Figure 2-1.

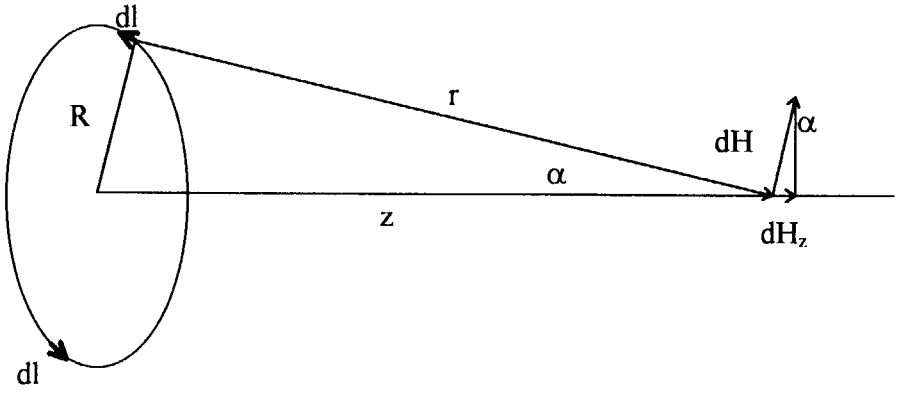

Figure 2-1.: Circular current carrying loop

The magnetic field in the axis of the circular loop will be evaluated starting from the Biot-Savart law, Eq.2.3. Considering just a small section of the coil its contribution can be expressed as

$$\overline{dH} = \frac{I}{4\pi}\frac{\overline{dl}\times\overline{r}}{r^3}$$

Its axial component is

$$dH_z = dH * \sin\alpha = dH\frac{R}{r} = I\frac{dl}{4\pi r^2}\frac{R}{r}$$

Integrating for the whole length finally we obtain

$$H = \oint dH_z = \frac{I}{4\pi}\frac{R}{r^3}2\pi r = \frac{I}{2}\frac{R^2}{r^3} = \frac{I}{2}\frac{R^2}{\left(R^2+z^2\right)^{3/2}}$$

2.2 Field distribution in the axis of a thin solenoid

Next let us consider an ideal cylindrical solenoid with radius R and length 2a as illustrated in Figure 2-2. Let N denote the number of turns.

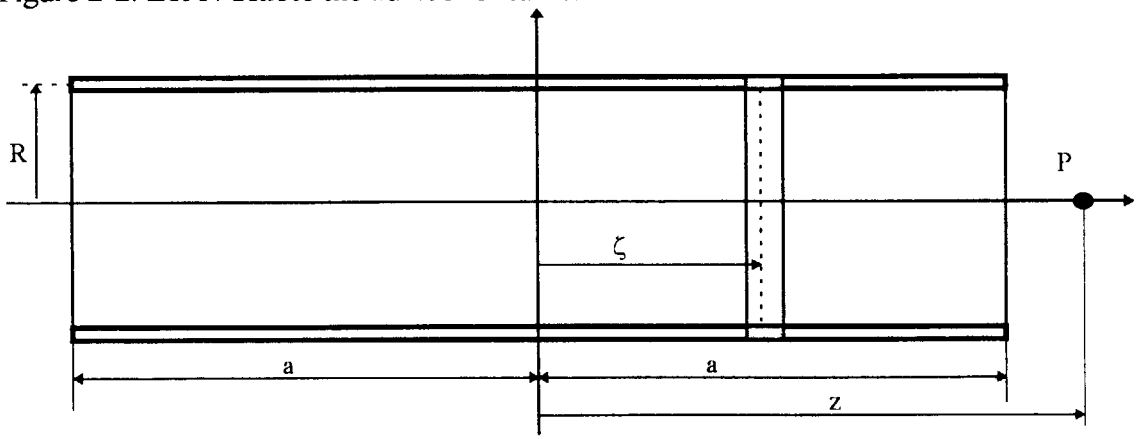

Figure 2-2.: Geometry of a thin solenoid

Based on the previous result the field produced by a small section with $d\zeta$ length is

$$dH = \frac{NI}{2a} d\zeta \frac{1}{2} \frac{R^2}{\left[R^2 + (z-\zeta)^2\right]^{3/2}}$$

The axial component of the magnetic field along the axis can be calculated by integration onto the total length

$$H(z) = \int_{-a}^{+a} \frac{NI}{4a} \frac{R^2}{\left[R^2 + (z-\zeta)^2\right]^{3/2}} d\zeta$$

Substituting $sh(t) = (z-\zeta)/R$ the final result is

$$H(z) = \frac{NI}{4a}\left[\frac{a-z}{\sqrt{R^2+(a-z)^2}} + \frac{a+z}{\sqrt{R^2+(a+z)^2}}\right]$$

This expression can be further simplified introducing α_1 and α_2 angles as illustrated in Figure 2-3:

$$H_z = \frac{NI}{2l}(\cos\alpha_1 - \cos\alpha_2)$$

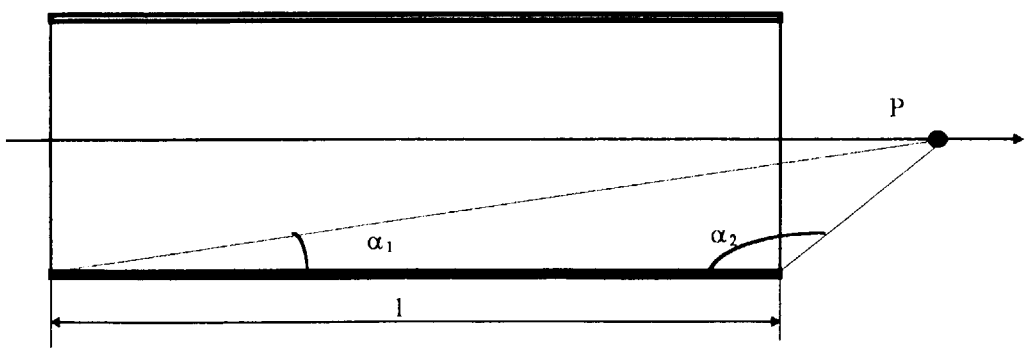

Figure 2-3.: Simplified notation

In the center the field intensity can be written as

$$H(0) = \frac{NI}{2\sqrt{R^2 + a^2}}$$

and at the end of the winding

$$H(\pm a) = \frac{NI}{2\sqrt{R^2 + 4a^2}}.$$

As an example the profile of the flux density along the axis of a solenoid is plotted in Figure 2-4 with the following parameters: a=0.9m, R=1.3m, N=540, I=46kA.

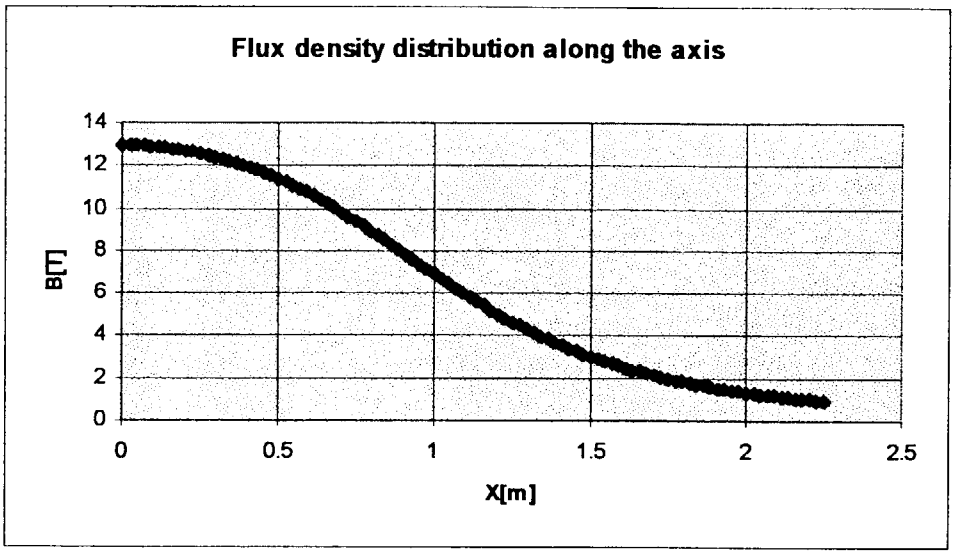

Figure 2-4.: Flux density profile in the axis of a thin solenoid

2.3 Field distribution in the entire cross-section of a current carrying circular loop

In this section the field distribution is determined in the cross-section of a cylindrical conductor by a semi analytical method after Simonyi [1]. Instead of the direct application of Biot-Savart law, the magnetic vector potential is introduced and we start from Eq.2.2. The magnetic vector potential has only azimuthal component A_φ because of the axial symmetry. The source point is denoted as (r',z') and the observation point as (r,z) in the following.

$$A_\varphi(r,z) = \frac{\mu_0 I}{4\pi} \oint_l \frac{\overline{dl}}{|\vec{r} - \vec{r'}|}$$

$$A_\varphi(r,z) = \frac{\mu_0 I}{4\pi} \int_0^{2\pi} \frac{r'\cos(\varphi'-\varphi)d\varphi'}{\sqrt{(z-z')^2 + r^2 + r'^2 - 2rr'\cos(\varphi'-\varphi)}}$$

Setting $\varphi = 0$

$$A_\varphi(r,z) = \frac{\mu_0 I}{4\pi} \int_0^{2\pi} \frac{r'd\varphi'\cos\varphi'}{\sqrt{(z-z')^2 + r^2 + r'^2 - 2rr'\cos\varphi'}}$$

Introducing a new variable $\beta = \dfrac{\pi - \varphi'}{2}$

$$\varphi' = \pi - 2\beta, \qquad d\varphi' = -2d\beta$$

$$\cos\varphi' = \cos(\pi - 2\beta) = -\cos 2\beta = 2\sin^2\beta - 1$$

$$\beta(\varphi' = 0) = \frac{\pi}{2}, \qquad \beta(\varphi' = 2\pi) = \frac{-\pi}{2}$$

$$A_\varphi(r,z) = \frac{\mu_0 I}{4\pi} r' \int_{\pi/2}^{-\pi/2} \frac{(2\sin^2\beta - 1)(-2)d\beta}{\sqrt{(z-z')^2 + r^2 + r'^2 - 2rr'(2\sin^2\beta - 1)}}$$

$$A_\varphi(r,z) = \frac{\mu_0 I}{2\pi} r' \int_{-\pi/2}^{\pi/2} \frac{(2\sin^2\beta - 1)d\beta}{\sqrt{(z-z')^2 + (r+r')^2 - 4rr'\sin^2\beta}}$$

$$A_\varphi(r,z) = \frac{\mu_0 I}{2\pi} \frac{r'}{\sqrt{(z-z')^2 + (r+r')^2}} \int_{-\pi/2}^{\pi/2} \frac{(2\sin^2\beta - 1)d\beta}{\sqrt{1 - \dfrac{4rr'\sin^2\beta}{\sqrt{(z-z')^2 + (r+r')^2}}}}$$

Introducing k^2 as

$$k^2 = \frac{4rr'}{(z-z')^2 + (r+r')^2}$$

$$A_\varphi(r,z) = \frac{\mu_0 I}{2\pi} \frac{r'}{\sqrt{(z-z')^2 + (r+r')^2}} \int_{-\pi/2}^{\pi/2} \frac{(2\sin^2\beta - 1)d\beta}{\sqrt{1 - k^2\sin^2\beta}}$$

The numerator can be reformulated as

$$2\sin^2\beta - 1 = \frac{2}{k^2} - 1 - \frac{2}{k^2}(1 - k^2\sin^2\beta) = \frac{2}{k^2}\left[\left(1 - \frac{k^2}{2}\right) - \left(1 - k^2\sin^2\beta\right)\right]$$

and the magnetic vector potential can be written as

$$A_\phi(r,z)=\frac{\mu_0 I}{2\pi}\frac{r'}{\sqrt{(z-z')^2+(r+r')^2}}\frac{2}{k^2}2\left[\left(1-\frac{k^2}{2}\right)\int_0^{\pi/2}\frac{d\beta}{\sqrt{1-k^2\sin^2\beta}}-\int_0^{\pi/2}\sqrt{1-k^2\sin^2\beta}\,d\beta\right]$$

Finally the magnetic vector potential can be expressed in cylindrical coordinate system as

$$A_\phi(r,z)=\frac{\mu_0 I}{2\pi}\frac{\sqrt{(z-z')^2+(r+r')^2}}{r}\left[\left(1-\frac{k^2}{2}\right)F\left(\frac{\pi}{2},k\right)-E\left(\frac{\pi}{2},k\right)\right]$$

where F() and E() are first and second order complete elliptic type integrals, respectively and

$$k^2=\frac{4rr'}{(z-z')^2+(r+r')^2}$$

$$F(k)=\int_0^{\pi/2}\frac{d\beta}{\sqrt{1-k^2\sin^2\beta}}$$

$$E(k)=\int_0^{\pi/2}\sqrt{1-k^2\sin^2\beta}\quad d\beta$$

The radial and the axial component of flux density formally can be obtained from the vector potential as

$$B_r(r,z)=-\frac{\partial A_\varphi}{\partial z}$$

$$B_z(r,z)=\frac{1}{r}\frac{\partial}{\partial r}(rA_\varphi)=\frac{A_\varphi}{r}+\frac{\partial A_\varphi}{\partial r}$$

Instead of the differentiation it is easier to derive expressions directly for B_r and B_z in similar way as for the vector potential. Without details the result can be written as follows:

$$B_r(r,z)=\frac{\mu_0 I}{2\pi}\frac{z}{r}\frac{1}{\sqrt{(r+r')^2+(z-z')^2}}\left[-F(k)+\frac{r^2+r'^2+(z-z')^2}{(r-r')^2+(z-z')^2}E(k)\right]$$

$$B_z(r,z)=\frac{\mu_0 I}{2\pi}\frac{z}{r}\frac{1}{\sqrt{(r+r')^2+(z-z')^2}}\left[F(k)+\frac{r'^2-r^2-(z-z')^2}{(r-r')^2+(z-z')^2}E(k)\right]$$

Unfortunately the above formulations are singular if r=0, therefore we apply the result obtained in Sec.2.2. in the axis:

$$A_\varphi(r=0,z):=0$$

$$B_r(r=0,z):=0$$

$$B_z(r=0,z):=\frac{\mu_0 I}{2}\frac{r'^2}{\left((z-z')^2+r'^2\right)^{3/2}}$$

2.4 Field distribution in the cross-section of a circular coil with rectangular cross-section

If the current distribution is given in the cross-section of a circular coil, the above formulation can be applied with enough fine discretization, summing up the contribution of individual sections.

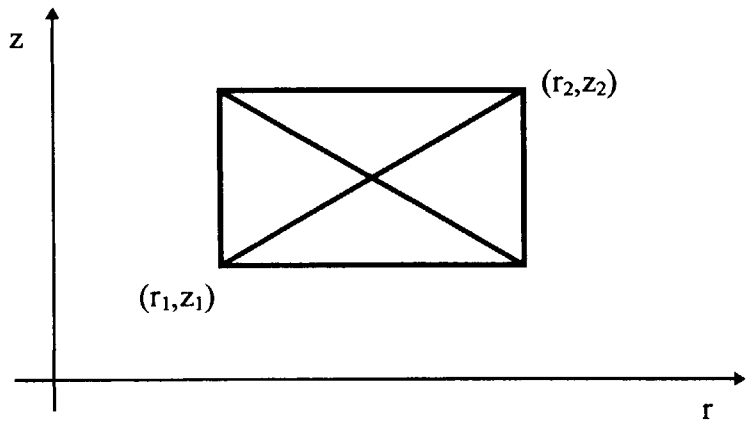

Figure 2-5.: Circular coil with rectangular cross-section

$$B_{r,coil}(r,z) = \int_{r_1}^{r_2} dr' \int_{z_1}^{z_2} \frac{J}{I} B_r(r,z,r',z')dz'$$

$$B_{z,coil}(r,z) = \int_{r_1}^{r_2} dr' \int_{z_1}^{z_2} \frac{J}{I} B_z(r,z,r',z')dz'$$

2.5 Integral formulations for nonlinear numerical evaluation

Iterative numerical solution is required if nonlinear magnetic properties are also considered. Here two methods are listed if the nonlinearity is given as single valued monotonous BH curve.

2.5.1 Magnetization current density

The simplest is to introduce a magnetization current density component in addition to the source current density by

$J_M = rot\, M$,

where

$$M = \frac{B}{\mu_0} - H .$$

To obtain the solution a simple iteration should be done applying the current density

$J = J_S + J_M$

to the elliptic integral method.

2.5.2 Solution method of Newman et al.

An alternative approach is worked out by Newman et al. which requires the iterative solution of the following integral equation

$$M(r) = \frac{\chi(r)}{4\pi}\left[\int_{\Omega_J} \frac{J(r') \times (r - r')}{|r - r'|^3} d\Omega' - \nabla \int_{\Omega_M} \frac{M(r')(r - r')}{|r - r'|^3} d\Omega'\right],$$

where M is the magnetization, J is the source current density and χ is the magnetic susceptibility. Instead of this formulation a 2D differential formulation will be used to study the magnetic behavior of Incoloy jacket.

2.6 Low frequency eddy current loss in a cylindrical rod

We consider a long cylinder made of ferromagnetic or non-ferromagnetic material. The flux density is supposed to be homogeneous and parallel to the axis. Moreover it is changing with a constant rate, $dB/dt = const.$ The induced electric field can be written as

$$\oint E_l(r) dl = -\frac{d\Phi}{dt}$$

on a radius r where

$$\frac{d\Phi}{dt} = r^2 \pi \frac{dB}{dt}.$$

Within the cylinder for $r < r_0$

$$E(r) = -\frac{r}{2}\frac{dB}{dt}.$$

Introducing ρ specific resistivity, the eddy current density J is given by

$$J(r) = -\frac{r}{2\rho}\frac{dB}{dt}.$$

The power loss per unit volume of the material is

$$\frac{P}{V}[W/m^3] = \frac{1}{\pi r_0^2}\int_0^{r_0} 2\pi r E(r) J(r) dr = \frac{1}{2\rho r_0^2}\left(\frac{dB}{dt}\right)^2 \int_0^{r_0} r^3 dr = \frac{r_0^2}{8\rho}\left(\frac{dB}{dt}\right)^2$$

The power loss is proportional to the square of the frequency. It also depends on the specific resistivity and the radius of the bar, however does not depend on the permeability as long as the flux penetration is complete.

As an example the eddy current power loss is evaluated due to the z-component of the field in inner tension rod. The total length of an inner tension rod is 4476mm and its diameter is 165mm. Only a short part of it (1775mm) is placed inside the coils. First the field profile is calculated along the tension rod. The conductivity is set to $\sigma = 2E6S/m$.
Substituting and integrating we obtain

$$P = \frac{Ar_0^2}{8\rho}\int_0^l \left(\frac{dB(z)}{dt}\right)^2 dz$$

A careful numerical integration results 53.2W power loss in one tension rod. This means 53.2W*13sec=692J energy loss in one tension rod during the energizing of magnet.

3. 3D Eddy Current Loss Calculation by FEM Using Differential Formulation

A domain consisting of a conducting sub-domain without current source and a non-conducting sub-domain with current source is considered.

3.1 Theoretical background

In present quasistatic case the following set of Maxwell's equations describes the field:

$$\nabla \times H = J \tag{3.1}$$

$$\nabla \times E = -\frac{\partial B}{\partial t} \tag{3.2}$$

$$B = \mu H \tag{3.3}$$

$$J = \sigma E \tag{3.4}$$

where σ denotes the conductivity. Its numeric value strongly depends on the temperature, which has to be considered. Following from eq.3.2 the magnetic flux density has to be solenoidal

$$\nabla B = 0. \tag{3.5}$$

Eq.3.1 implies that

$$\nabla J = 0. \tag{3.6}$$

In practice this means that at interfaces between air and metal no normal component of current is present. The eddy current analysis is carried out using magnetic vector potential **A**, introduced by means of the relation

$$B = \nabla \times A \tag{3.7}$$

satisfying identically eq.3.5. Introducing a scalar potential V, eq.3.2 is satisfied by defining the electric field intensity as

$$E = -\frac{\partial A}{\partial t} - \nabla V. \tag{3.8}$$

The governing equation for A and V in the eddy current region can be obtained from eqs. 3.1, 3.7 and 3.8:

$$\nabla \times \frac{1}{\mu} \nabla \times A + \sigma \frac{\partial A}{\partial t} + \sigma \nabla V = 0. \tag{3.9}$$

In order to define A uniquely the Coulomb gauge is applied

$$\nabla A = 0. \tag{3.10}$$

ANSYS [5] replaces eq.3.9 by

$$\nabla \times \frac{1}{\mu} \nabla \times A - \nabla \frac{1}{\mu} \nabla A + \sigma \frac{\partial A}{\partial t} + \sigma \nabla V = 0. \tag{3.11}$$

after Biro [6] and in order to satisfy the solenoidal requirement

$$\nabla \sigma \left(\frac{\partial A}{\partial t} \right) + \nabla V = 0$$

is imposed. The non-conducting region is represented with the simple formula

$$\nabla \times \frac{1}{\mu} \nabla \times A = J_S \tag{3.12}$$

where J_S is the source current density. An alternative approach is to use magnetic scalar potential in the non-conducting region. In such a case the normal component of **A** also should be specified on the interface by the constraint

$A \cdot n = 0,$
for the unique solution.

3.2 Boundary and Interface Conditions

Flux-normal boundary conditions can be satisfied by setting the normal component of **A** to zero. Flux-parallel conditions has to be satisfied setting the in-plane components of **A** to zero. For far-field simulation infinite elements has to be used. Periodic or cyclic symmetry can be satisfied prescribing constraint equations or coupling the nodes. An imposed external field requires to set A_x, A_y, A_z values to the necessary one. Finally a numerical value for V must be fixed somewhere within the conducting region.

3.3 Post-processing

The current density is calculated over all of the finite elements where the conductivity is different from zero. Next the power loss per unit volume is calculated and integrating for the total volume the power loss is obtained as

$$P(t) = \int_V \rho \left[J(t) \right]^2 dv \quad [Watt].$$

Integrating according to the time, the energy loss (Joule heat) can be written as

$$E(t) = \int_0^t P(\tau) d\tau \quad [Joule].$$

3.4 Time derivative

If the solution is done in the time domain, the following simple scheme can be used

$$\Theta \dot{A}^{k+1} + (1 - \Theta) \dot{A}^k = \frac{A^{k+1} - A^k}{\Delta t},$$

where index k notes the previous solution step and k+1 the new solution step. The time step Δt should be enough small and constant Θ larger than 1/2 for a stable solution. We will use Θ=2/3.

4. 2D Differential Formulation

2D differential formulation will be applied to the eddy current loss calculation of Incoloy jackets in cylindrical coordinate system. The differential formulation of 2D problems is widely used, therefore we do not repeat the derivations. However some remarks will be done on axisymmetric problems and current force.

4.1 Current Force in 2D

The one component magnetic vector potential is selected to describe the 2D eddy current problem. The governing equation can be written as

$$\nabla \times \frac{1}{\mu} \nabla \times A = J_S - \sigma \dot{A},$$

where J_S is the source current density. This formulation provides only voltage forced solution. If the total current has to be prescribed in the cross-section (current force) than the source current term should be substituted [7] by

$$J_S = \frac{I + \int_{T_{Conductor}} \sigma \frac{\partial A}{\partial t} dS}{T_{Conductor}}$$

where $T_{conductor}$ denotes the area of the cross-section of conductor in which the current should be prescribed.

This is the situation in case of Incoloy jacket which carries only eddy currents, but the total current should be zero in the whole cross-section. Note, that the assembled matrix will include long lines at vector potential values belonging to the jacket. This slows down the solution procedure and also requires additional storage capacity.

4.2 Solution in Cylindrical Coordinate System

The energy related functional for axisymmetric problems is

$$W(A) = 2\pi \int_{\Omega} \left\{ r \left[\frac{1}{\mu} \left(\frac{\partial A_\varphi}{\partial z} \right)^2 + \frac{1}{\mu} \left(\frac{\partial A_\varphi}{\partial r} \right)^2 - 2 J_S A_\varphi + \sigma A_\varphi \dot{A}_\varphi \right] + \frac{2}{\mu} A_\varphi \frac{\partial A_\varphi}{\partial r} + \frac{1}{\mu} \frac{A_\varphi^2}{r} \right\} d\Omega$$

There is a singularity in r=0, causing problem during the numerical solution. To eliminate the singularity the modified vector potential should be introduced as follows

$$A_\varphi' = \frac{A_\varphi}{\sqrt{r}} \quad \text{or} \quad A_\varphi'' = \frac{A_\varphi}{r}.$$

In this case

$$W(A) = 2\pi \int_{\Omega} r^2 \left[\frac{1}{\mu} \left(\frac{\partial A_\varphi'}{\partial z} \right)^2 + \frac{1}{\mu} \left(\frac{\partial A_\varphi'}{\partial r} \right)^2 \right] d\Omega + \frac{9}{4\mu} \int_{\Omega} \left(A_\varphi' \right)^2 d\Omega + \frac{2}{\mu} \int_{\Omega} r A_\varphi' \frac{\partial A_\varphi'}{\partial r} d\Omega -$$

$$- 2 \int_{\Omega} \sqrt{r} A_\varphi J d\Omega + \sigma \int_{\Omega} r A_\varphi \dot{A}_\varphi d\Omega$$

An other way is to select integration points far enough from the axis during finite element processing. The solution in node points can be obtained by extrapolating the results obtained in integration points.

5. AC Loss of Superconducting Cables

If an external field is applied to a bulk Type-II superconductor screening currents will appear. The change of external field results hysteresis loss because the screening currents do not decay themselves due to the zero resistance of supeconductor.

Under some condition the critical state of a superconductor may be unstable, because flux motion generates heat and the critical field depends on the temperature. They may cause flux jump by positive feedback, which results in the loss of superconducting state abruptly. Against flux jump fine filaments should be composed. Superconducting hysteresis loss also decreases if fine filaments are applied. In the practice for magnet winding filamentary composites are used in which the fine filaments are embedded in a matrix of normal metal (usually copper) having good electrical conductivity. The good ductility of copper allow us to wind a magnet, the good electrical conductivity along the strand also give protection against flux jump and protect the conductor from burn-out if the magnet quenches. However the good conductivity of copper matrix cause the coupling of filaments together in changing magnetic field by cross-over eddy currents, resulting in coupling loss. Due to coupling the superconducting hysteresis loss also increases, since the whole strand will behave like a thick superconductor. The coupling can be significantly decreased by twisting the filaments. In addition we have to find an optimum choice of electrical conductivity which is a compromise between the conflicting demands of low A.C. loss and good stability. In many case resistive alloy jacket is placed around each filament to increase the cross-over resistivity and hence decrease the coupling loss, but keep the good conductivity along the strand.

The transport current itself produce a self-field. This is why the current flow is located in an outermost shell.

From the strands conductors are constructed. The lager the magnet the lager the conductor in order to be protected during quenching. Strands are twisted together to reduce the magnetic coupling between them. They are also fully transposed to minimize a self-field effect.

5.1 Characterization of Superconductors

To describe superconductivity several physical models were developed:

- 1935 London theory
- 1950 Ginzburg-Landau theory
- 1957 BCS theory (Barden-Cooper-Schrieffer)

There are also simple models used successfully in engineering. They use the E-J constitutive equation. Here just a brief summary is given.

5.1.1 Critical state models

Bean model applies an idealized E-J relationship

$$J = J_c \frac{E}{|E|} \quad if \quad E \neq 0 \quad \text{and}$$

$$\frac{dJ}{dt} = 0 \quad if \quad E = 0,$$

generally referred as critical state model.

Kim-model also takes into consideration the critical current density dependence on the field as

$$J_c = \frac{J_{c0}}{B + B_0}$$

where J_{c0} and B_0 are constants.

Yasukochi model use an other relationship for the critical current density dependence

$$J_c = \frac{J_{c(B=1T)}}{\sqrt{B}}$$

5.1.2 Flux flow and creep model

$$E = f(|J|)\frac{J}{|J|}$$

and

$$f(J) = 2E_c \sinh\left(\frac{U_0}{kT}\frac{J}{J_c}\right)\exp\left(\frac{-U_0}{kT}\right) \quad if \quad J < J_c$$

$$f(J) = \rho_c J_c + \rho_f (J - J_c) \quad if \quad J > J_c$$

where ρ_f and ρ_c denotes the flow and creep resistivity respectively while U_0 is the pinning potential.

5.2 Superconducting Hysteresis (characterization by BH-loop)

In the following the hysteresis of superconductors is demonstrated. Let us consider a superconducting slab of thickness 2a which is placed into H_e external magnetic field. The average flux density above the slab can be written as

$$B = \frac{\mu_0}{2a}\int_0^{2a} H(x)dx$$

and the equivalent magnetization of the slab is

$$M = \frac{B}{\mu_0} - H_e .$$

For the calculation of the magnetization, we should know the magnetic field distribution within the slab. The externally applied magnetic field induce a persistent current in the superconductor. Based on the critical state model the current density distribution has a rectangular profile in shape resulting a linear profile of magnetic field within the slab. In general $rotH = J$ should be applied, which is simplified now to

$$e_z \frac{dH_y}{dx} = -J_{z,c}$$

Increasing the magnetic field from zero to H_e value, the penetration depth is given by

$$\delta = \frac{H_e}{J_c} .$$

To achieve full penetration δ=a an external field with amplitude

$$H_p = J_c a$$

should be applied. The flux density over the slab in case of full penetration is

$$B_p = \frac{\mu_0}{2a} 2\int_0^a J_c x dx = \frac{\mu_0 J_c a}{2} .$$

The magnetization of the slab can be written as

$$M_p = \frac{B_p}{\mu_0} - H_p = \frac{J_c a}{2} - J_c a = -\frac{J_c a}{2} = -\frac{H_p}{2} .$$

Increasing the field from a virgin state up to a maximum value $H_{max}<H_p$ and next decreasing back to zero, the average flux density is lager than zero. The changes of the field profile is summarized in Figure 5-1 for increasing and decreasing external magnetic field.

In CS Model Coil a cyclic trapezoidal unidirectional excitation current is applied which also produces a cyclic unidirectional magnetic field. The maximum value of the field is over the full penetration. Flux profiles within a slab superconductor under the same excitation conditions are plotted in Figure 5-2.

In case of a cylinder perpendicular to the field the external field necessary to achieve full penetration is

$$H_p = \frac{4J_c a}{\pi}$$

and the magnetization is

$$M_p = -\frac{4J_c a}{3\pi} .$$

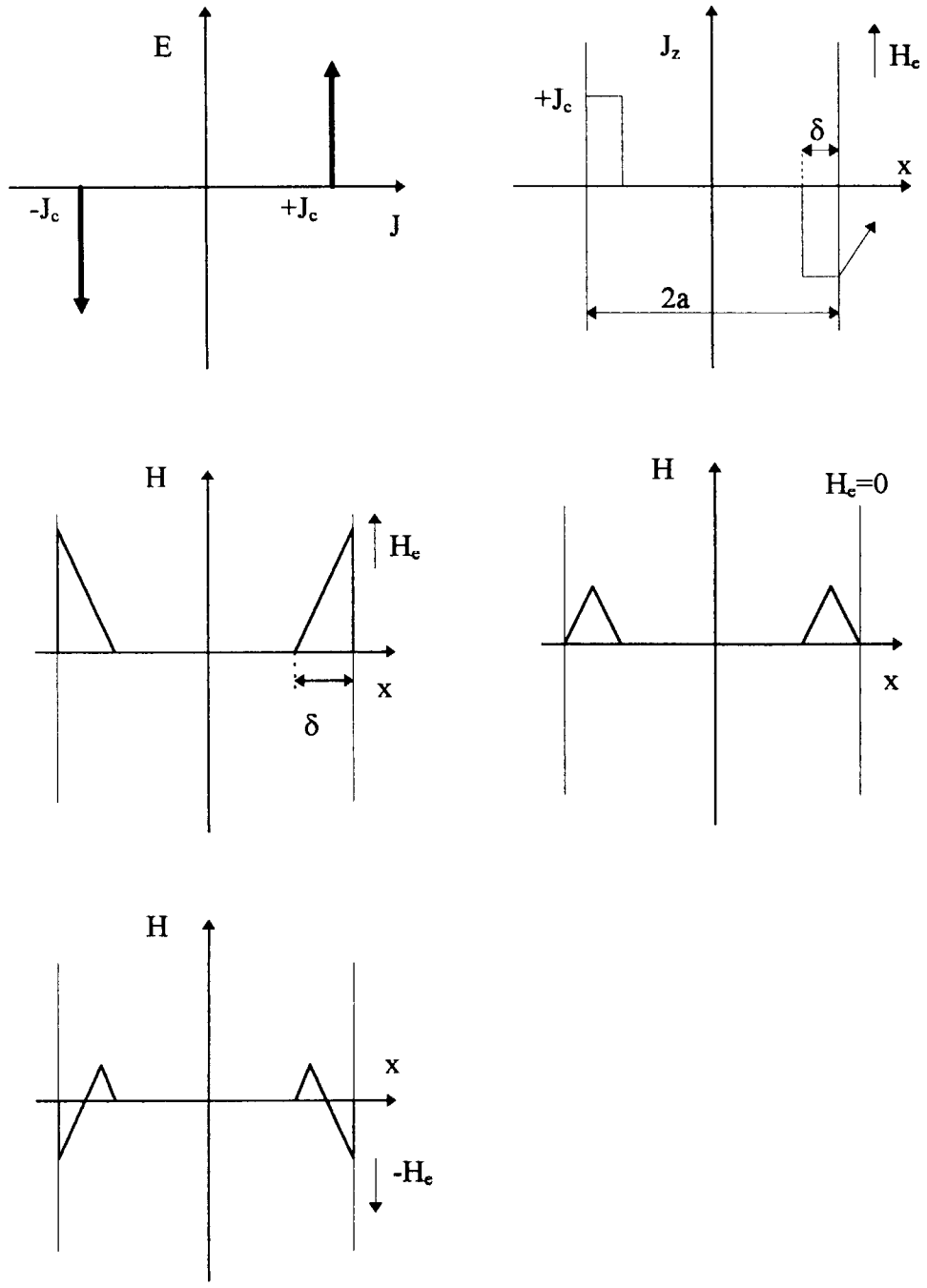

Figure 5-1.: A virgin Bean-slab placed into increasing and decreasing magnetic field

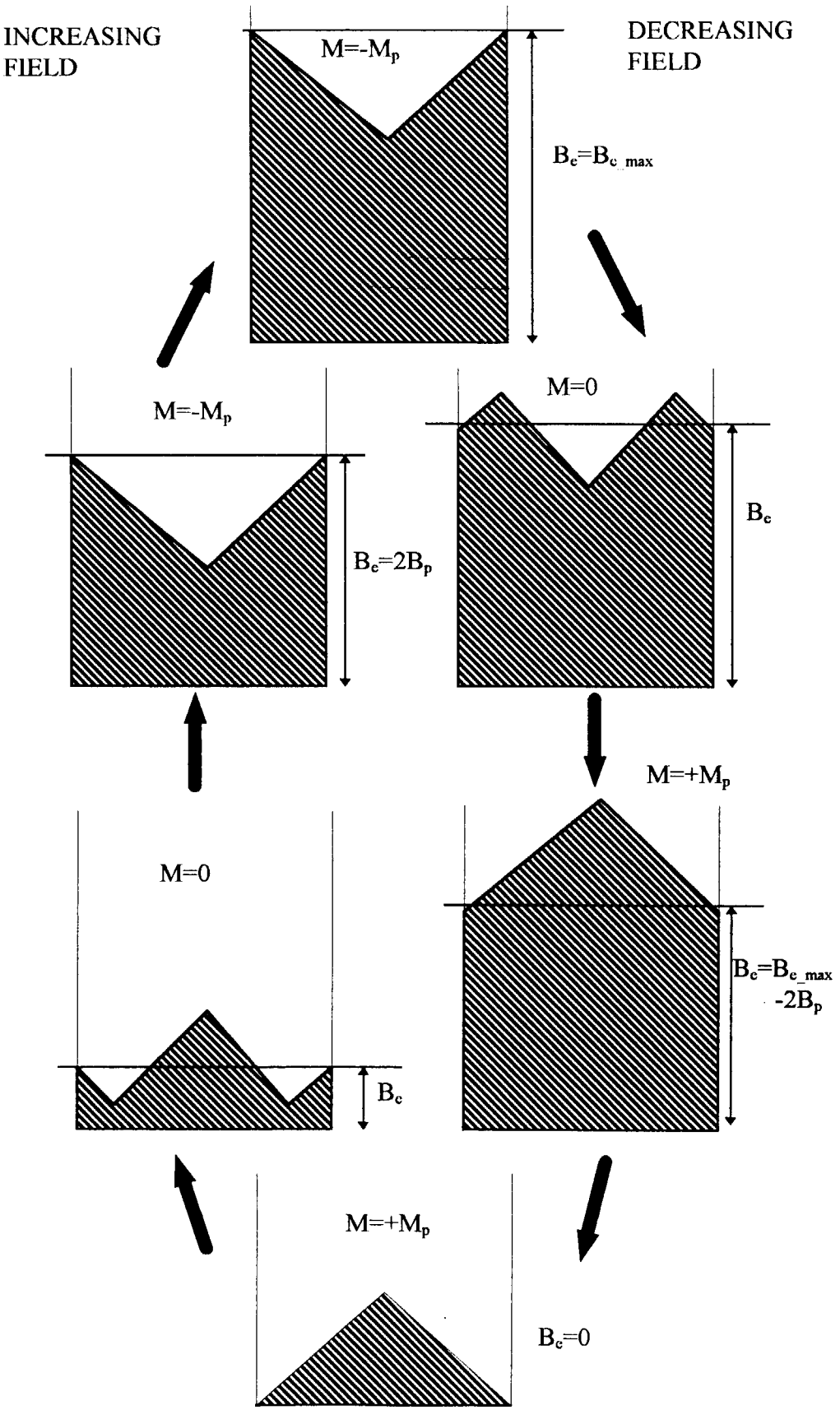

Figure 5-2.: Cyclic magnetization of a slab superconductor based on Bean model

5.3 Superconducting hysteresis loss

The energy loss caused by superconducting hysteresis can be evaluated by the help of Pointing vector

$$-\oint\int_S \overline{E}\times\overline{H}dsdt = \int\oint_V \overline{EJ}dtdv + \mu_0\int\oint_V \overline{HdM}\,.$$

Where S is the surface of the V volume under interest. After some manipulation the energy loss over a full cycle can be expressed as

$$Q = -\mu_0\oint MdH_e\,.$$

The energy loss per unit volume for cylinders over full penetration can be evaluated by the formula [2]

$$Q = \frac{8}{3\pi}J_c a B_m,$$

where B_m is the amplitude of a fully reversed cyclic external field. The critical current density dependence on the magnetic field has to be also considered.

5.4 Coupling loss in transverse field

The coupling loss depends on the twist pitch length and the effective matrix resistivity, since they determine the time constant of the system, and also depends on the excitation. The time constant can be written as [2]

$$\tau = \frac{\mu_0}{2\rho_{et}}\left(\frac{L}{2\pi}\right)^2$$

Usually it is determined from measurements since it is difficult to calculate the effective matrix resistivity. If a trapezoidal excitation signal is applied with maximum value B_m and ramp up time T_m which is large comparing to τ, than the power loss and energy loss per unit volume can be calculated from [2]

$$\frac{P_c}{V} = \frac{B_m^2}{T_m^2}\frac{1}{\rho_{et}}\left(\frac{L}{2\pi}\right)^2 = \frac{2B_m^2}{T_m^2\mu_0}\tau$$

$$\frac{Q_c}{V} = \frac{4B_m^2}{\mu_0}\frac{\tau}{T_m}$$

These loss formulas are derived with some ideal assumptions. In the practice the external layer of filaments carries critical current density and this zone propagates toward the inner part of strands if it is necessary. The loss produced during propagation is called penetration loss. This component of loss is not considered now.

5.5 Self-field loss

Even if the filaments are well twisted and the coupling is reduced between them, the transport current itself produce a circular field around the conductors which is associated with energy loss as well. The only method to decrease self field loss is to fully transpose filaments and strands. Also strand diameter should be small, presently it is 0.81 mm.

5.6 Summary

In pulsed magnets the filaments should be as fine as possible because of two reasons. First to avoid flux-jumping, second to decrease superconducting hysteresis loss. The transverse resistivity of the embedding copper matrix should be as high as possible in order to decrease coupling loss. On the same time conductivity in the longitudinal direction must be high to provide dynamic stability and to protect magnet during quenching. The AC loss of twisted superconducting filamentary composits consist of

I. superconducting hysteresis loss (the critical current density dependence on magnetic field and the transport current should be considered),
II. coupling loss (current through the copper matrix, current through the peripheral layer of strand and eddy current in the peripheral layer),
III. penetration loss and
IV. self field loss.

5.7 Measuring the loss

We can not measure the components of loss of a superconducting cable, only the total loss. Generally calorimetric method is used and calibrated with a resistive heater. In the practice the largest amount of loss consists of coupling loss and superconducting hysteresis loss. Other components may be neglected. The energy loss can be written as

$$Q = Q_H + Q_C = c_1 B_m + c_2 B_m \dot{B} \tau$$

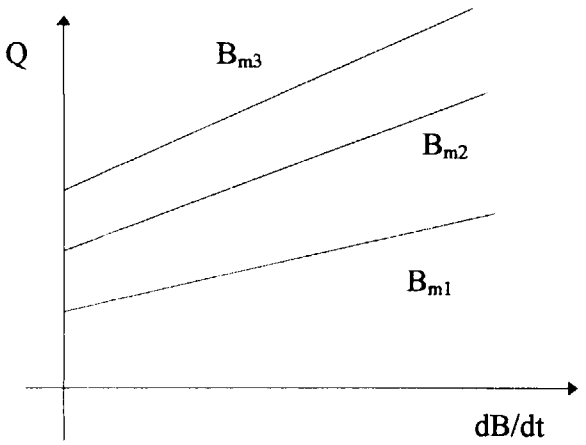

Figure 5-3.: Energy loss dependence on flux change rate and maximum value of applied external magnetic flux density ($B_{m1}<B_{m2}<B_{m3}$)

This is a blank page.

Part B
Calculation Results

This is a blank page.

1. Introduction

The Central Solenoid (CS) Model Coil is designed to produce magnetic field with maximum flux density of 13T in case of 46kA excitation current. The coil will operate in "pulse mode". Present interest is to determine the total heat-loss produced in different parts of the magnet, namely the eddy current loss of supporting structures, the AC loss of superconducting cables (including the superconducting hysteresis loss of Nb_3Sn filaments, eddy current loss, coupling loss), the ferromagnetic hysteresis and eddy current loss of Incoloy jackets. Also the analysis of butt-type and lap-type joints is necessary. The produced loss can be categorized as follows:

- Eddy current loss in Cu, Incoloy, stainless steel and other metal structures
- Superconducting Hysteresis loss in Nb_3Sn material
- Ferromagnetic Hysteresis loss in Incoloy

1.1 Basic Consideration

In order to calculate the AC loss of superconductors, the eddy current loss and the ferromagnetic hysteresis loss of the magnet,

$$W_{total}(B_{total}) = W_{eddy\_current}(B_{total}) + W_{SC}(B_{total}) + W_{Fe\_Hysteresis}(B_{total}),$$

the total magnetic flux density (B_{total}) will be decomposed into two components; an ideal one (B_{ideal}) and a perturbed component ($B_{perturbed}$). The ideal component is generated by an ideal coil while the perturbed component is produced by eddy currents, superconducting hysteresis and ferromagnetic hysteresis phenomena:

$$B_{total}(B_{ideal}, B_{perturbed}) = B_{ideal} + B_{perturbed}(B_{ideal})$$

Neglecting the perturbed part of the flux density we may receive a good approximation of the loss. (Not the ferromagnetic hysteresis or other phenomena are neglected but only their contribution to the magnetic field.) The advantage of this simplification is, that we can consider the components by one by one interacting with the ideal field component and finally obtain the total loss by summing up the contribution of individual parts. A simple calculation can show, that the contribution of low frequency eddy currents to the perturbed field can be really neglected. The contribution of ferromagnetic behavior will be discussed.

1.2 Components of CS Model Coil (Electromagnetic Model)

The arrangement of winding and metal components of supporting structure are plotted in Figure 1-1 and Figure 1-2. The winding consist of modules, namely Inner Module-A, Inner Moule-B and Outer Module. In addition an Insert Coil is also placed inside. Two grades of conductor are used. In Insert Coil and in Inner Module-A where the magnetic field is high CS1-type conductor is used, while in Inner Module-B and in Outer Module CS2-type conductor is applied.

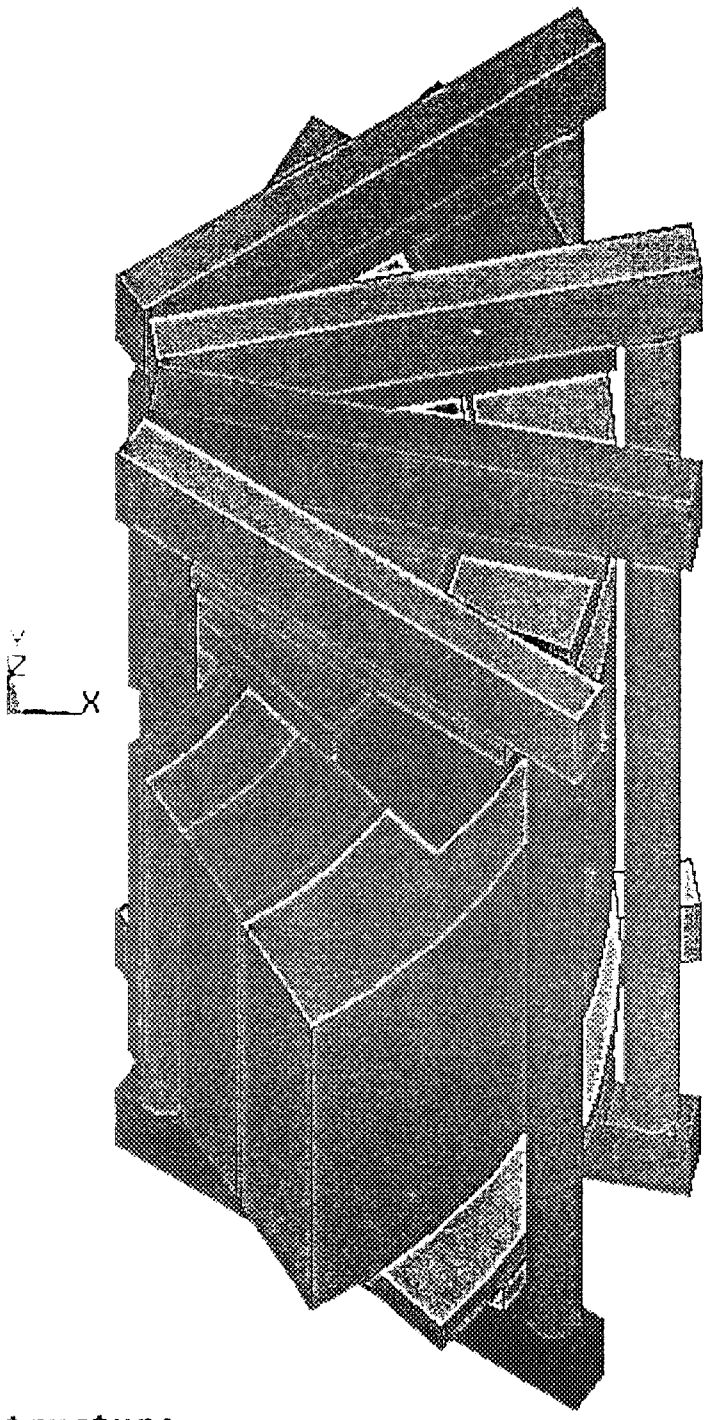

Figure 1-1.: Arrangement of Winding of CS Model Coil

The supporting structure is manufactured from SS316 stainless steel. Figure 1-2 illustrates one quarter of the structure without the winding. There are totally 16 inner and 16 outer tension rods in contact with 16 upper and 16 lower tension beams. Below tension beams tension plates are located. The lower plate support consist of 4 segments, called Lower tension plates hereafter. They are the most critical because of their large size. The upper side is much more divided, consisting of 8 upper-inner tension plates and 16 upper-outer tension plates.

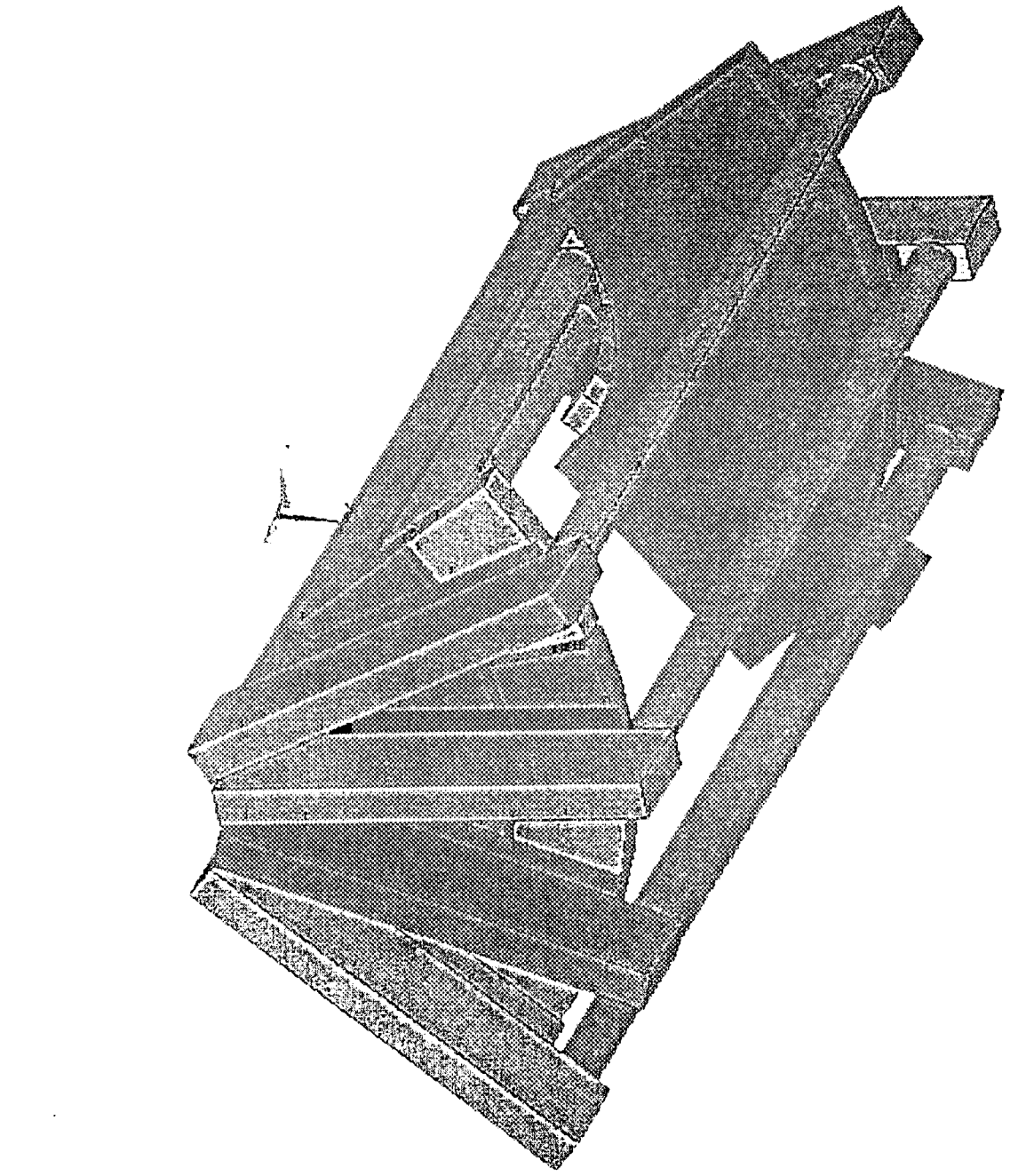

Figure 1-2.: Arrangement of metal components of the supporting structure

2. Magnetic Field Distribution

The major geometric parameters of winding and the maximum values of applied excitations are listed in Table 2-1. First the distribution of magnetic flux density is calculated in the cross-section of the model coil and plotted for the center line in Figure 2-1. Next a simplification is introduced. Instead of the complicated structure of Insert coil, Inner module and Outer module, a simple solenoid is used with homogeneous source current distribution. Its inner diameter is selected to be R_i=0.785m, its outer diameter R_o=1.81m and its height h=1.775m. The maximum value of excitation current density is set according to Table 2-2 to produce the same field in the center, as it is in the case of detailed model. The field profile produced by the simplified solenoid is plotted in Figure 2-2. Within the winding there is some difference between the two profiles.

Table 2-1.: Major parameters of winding

	Insert Coil	Inner Module		Outer Module
Kind of Conductor	CS1	CS1	CS2	CS2
Inner Radius	0.716m	0.8m	1.0315m	1.377m
Outer Radius	0.77m	1.0315m	1.347m	1.79m
Height	1.81m	1.6596m	1.6828m	1.67776m
Layer Numbers	1	4	6	8
Turn Numbers	30.875	122.9375	206.0625	273.92
Current per turn	40kA	46kA		46kA
Average Current Density	14.53MA/m^2	14.72MA/m^2	17.85MA/m^2	18.1845MA/m^2

Table 2-2.: Maximum current density of simplified coil

	With Insert Coil	Without Insert Coil
B_{center}	12.137T	11.404T
J_{max}	16.396 MA/m^2	15.405 MA/m^2

Both r and z-component of the flux density are plotted along inner tension rod in Figure 2-3, along outer tension rod in Figure 2-4 and along tension beam in Figure 2-5.

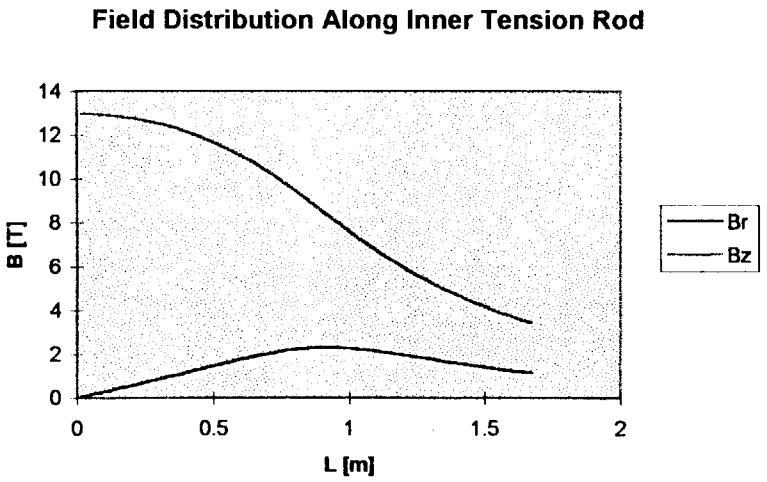

Figure 2-3

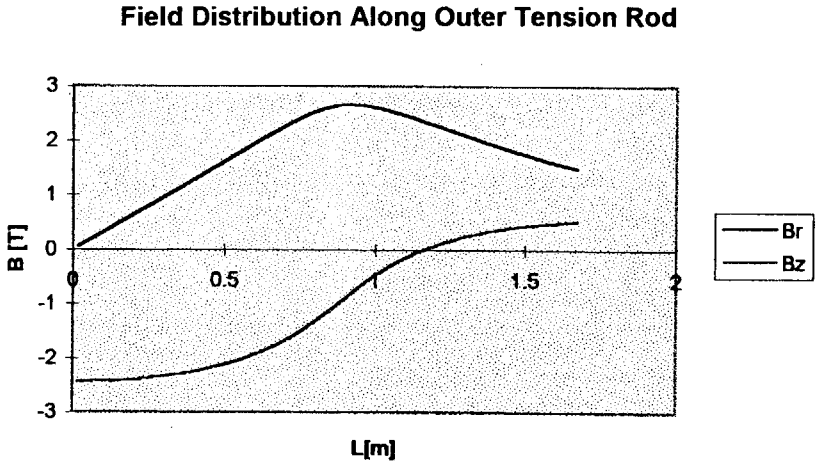

Figure 2-4

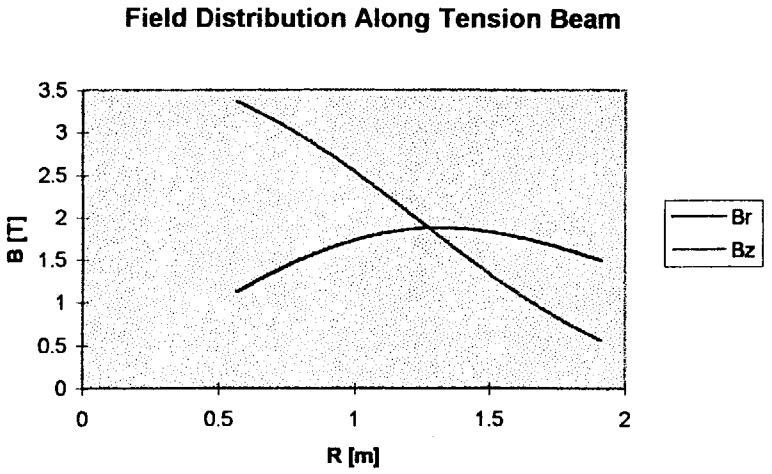

Figure 2-5

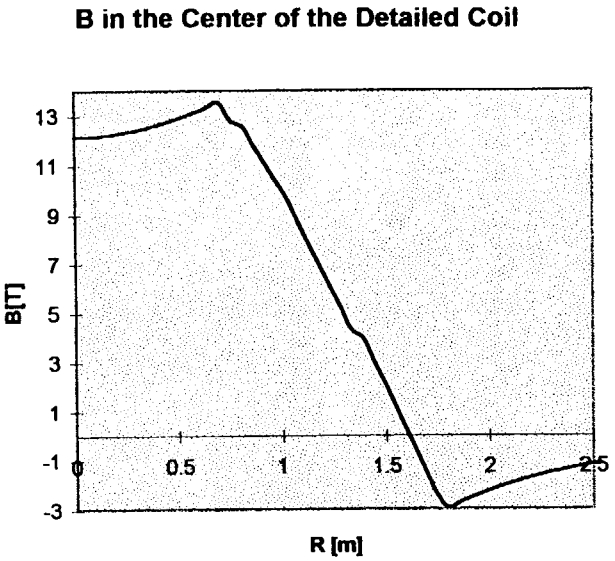

Figure 2-1.: Field profile produced by the detailed coil

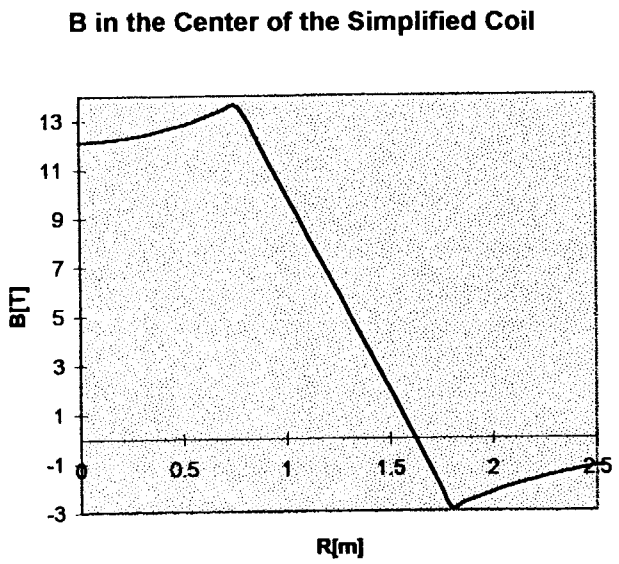

Figure 2-2.: Field profile produced by the simplified solenoid

3. Eddy Current Loss in Structural Components

The heat loss produced by eddy currents is calculated in the following components:

- inner tension rods
- outer tension rods
- upper tension beams
- lower tension beams
- upper-inner tension plates
- upper-outer tension plates
- lower tension plates

The governing equation of the quasistatic electromagnetic problem is expressed in terms of the magnetic vector and electric scalar potentials. The numerical calculation is done by 3D ANSYS/EMAG code. Only single components are considered, since it is supposed, that they are electrically insulated from each other. Since the specific resistivity of metal strongly depends on the temperature, a wide resistivity range is considered. However the temperature distribution is not taken into account within rods.

For our convenience the current and current density change rates are defined as follows

$\frac{dI}{dt} = n*\left(\frac{46kA}{13\,\mathrm{sec}}\right)$ in Inner and Outer module

$\frac{dI}{dt} = n*\left(\frac{40kA}{13\,\mathrm{sec}}\right)$ in Insert Coil

$\frac{dJ}{dt} = n*\left(\frac{16.396MA}{13m^2\,\mathrm{sec}}\right)$ in the simplified solenoid

where n is the excitation rate factor. The calculations are done for n=1. The results can be recalculated for other specific resistivity values or excitation rate factor n if the current distribution is not changed by the formula

$$P = \frac{const.}{\rho} n^2 .$$

3.1 Eddy Current Loss in Electrically Insulated Components

The assumptions and conditions for the numerical analysis were the following:

- The specific resistivity is lager than $[10^{-8}\,\Omega m]$
- The specific resistivity distribution is homogeneous
- The magnetic property of Incoloy is not considered
- Only one metal component is present in every time
- The current increases linearly in time and n=1 or n=1.07922
- The simplified solenoid is used instead of the detailed one

Only the upper half of the CS model coil is considered because of the symmetry in axial direction. The model coil is placed in the center of a global cylindrical coordinate system in such a way that the axis of the solenoid is fitted to the z-axis and the origo is in the half symmetry plane. Moreover the $\varphi = 0$ plane fits to the axis of an arbitrary chosen tension rod. The problem is cyclic in such that a slice of 22.5^{O} degrees between $\phi = -11.25°$ and $\phi = 11.25°$ can be selected.

Tetrahedral elements with midpoints are used. The element type is SOLID97 with AX,AY,AZ and VOLT degrees of freedom in the metal and AX, AY and AZ DOF in the air. INFIN111 elements are used to model the infinite region with AX, AY and AZ DOF. The source current density as a body force is prescribed after rotating the element coordinate systems parallel to the global cylindrical one.

Instead of the periodic boundary condition at the $\phi = -11.25°$ and $\phi = 11.25°$ degree planes, flux-parallel conditions are applied. This deforms only the field produced by eddy currents. This effect is small. Flux-normal conditions are applied at the z=0 plane. All of the flux parallel and perpendicular conditions are prescribed in the rotated nodal coordinate systems. At the axis AX, AY and AZ are set to zero. The external nodes of the infinite surface are marked by infinite surface flags. In one node of the tension rod the time integrated scalar potential is set to zero.

The power loss and energy loss are calculated by the time history post-processor.

The eddy currents in tension rods behave like the current of a voltage forced RL-circuit. Therefore switching transients occur. The eddy current calculation is terminated after reaching the stationer power loss value.

3.1.1 Tension Rods

Table 3-1 Results of 3D ANSYS analysis

	n=1	n=1.07922	Specific resistivity
Inner tension rod	3248W	3783W	$10^{-8}\Omega m$
Inner tension rod	32.48W	37.83W	$10^{-6}\Omega m$
Outer tension rod	535W	622W	$10^{-8}\Omega m$
Outer tension rod	5.35W	6.22W	$10^{-6}\Omega m$

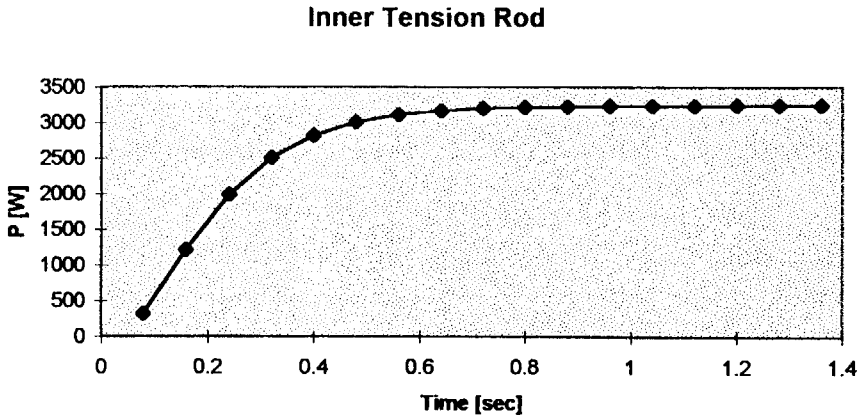

Figure 3-1.: Time dependence of power loss in tension rod

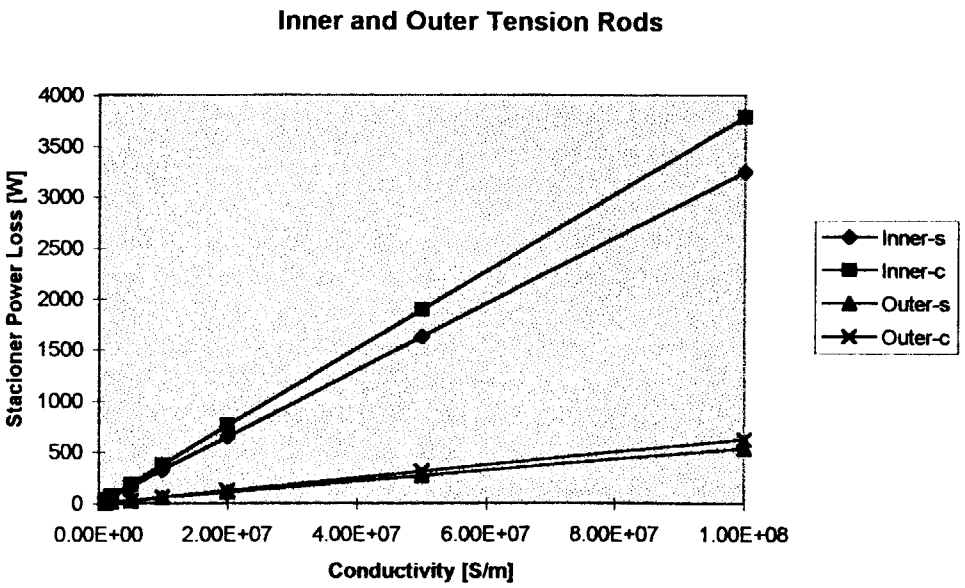

Figure 3-2.: Power loss vs. conductivity in tension rods

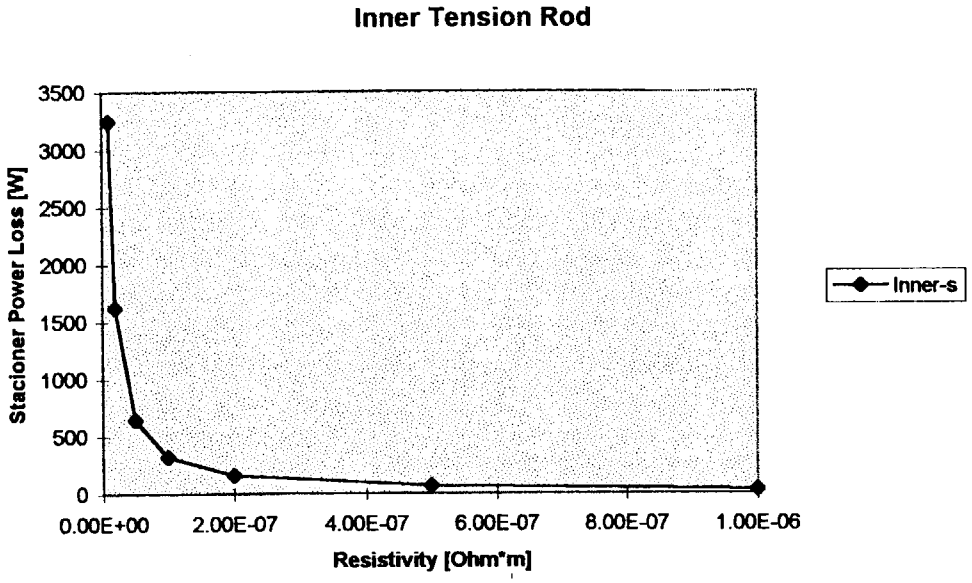

Figure 3-3.: Power loss vs. resistivity in inner tension rod

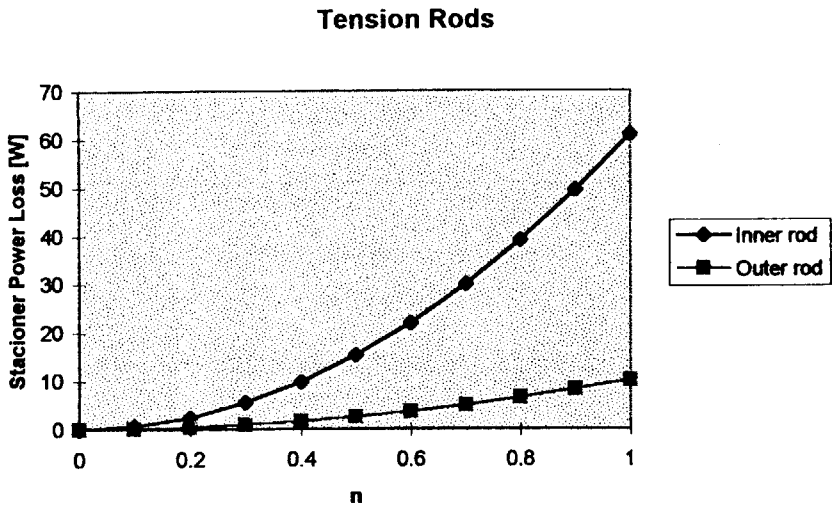

Figure 3-4.: Power loss dependence on flux change rate in tension rods

Table 3-2 Equations to calculate power loss for specific resistivity values larger than $10^{-8}\Omega m$

Inner tension rod	$P = 3.248*10^{-5}\sigma * n^2 = \frac{3.248*10^{-5}}{\rho} * n^2$, if n≤1
Outer tension rod	$P = 5.35*10^{-6}\sigma * n^2 = \frac{5.35*10^{-6}}{\rho} * n^2$, if n≤1

3.1.2 Tension Beams

Table 3-3 Results of 3D ANSYS analysis of tension beams

	n=1	n=1.07922	Specific resistivity
Upper tension beam	733W	854W	$10^{-8}\Omega m$
Lower tension beam	677W	789W	$10^{-8}\Omega m$

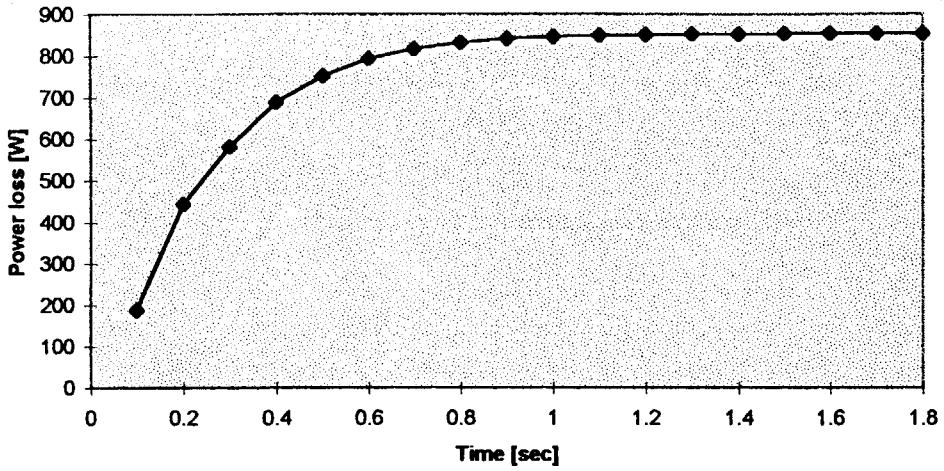

Table 3-4 Power loss as a function of time produced in upper tension beam ($\rho = 10^{-8}\Omega m$)

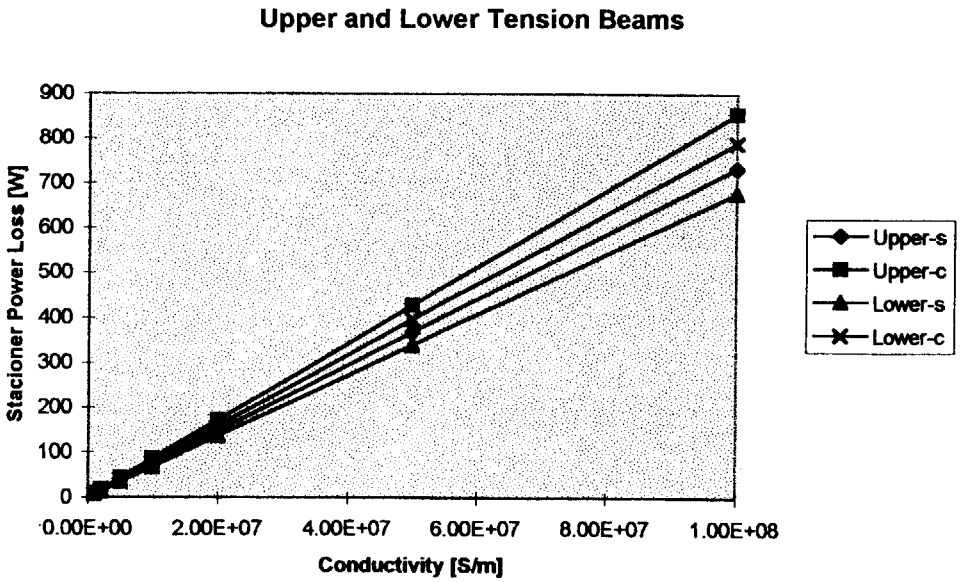

Figure 3-5.: Power loss dependence on conductivity in tension beams

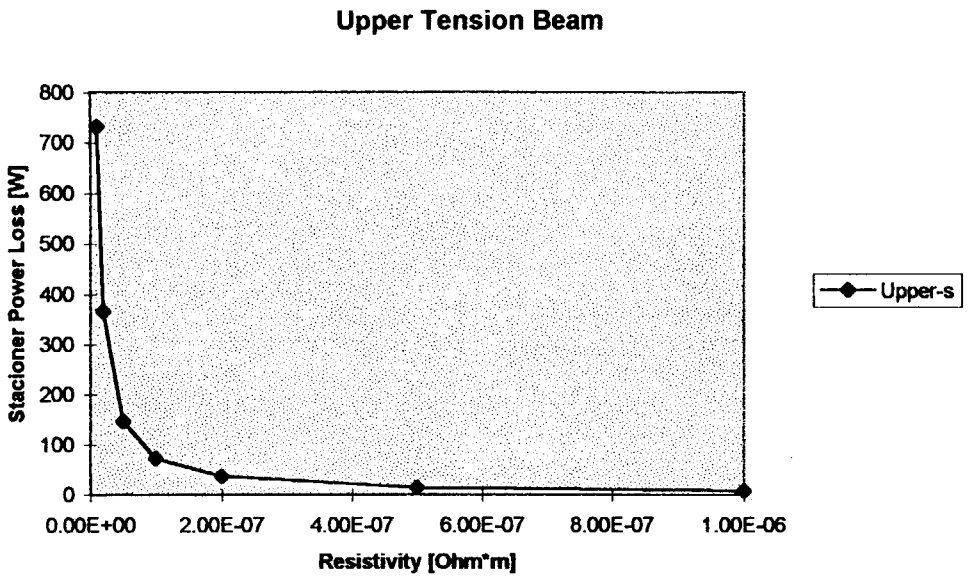

Figure 3-6.: Power loss dependence on specific resistivity in upper tension beam

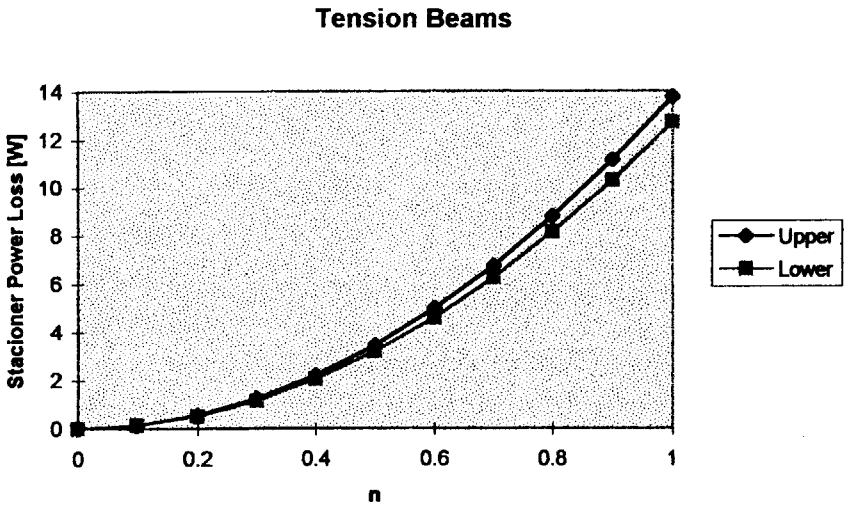

Figure 3-7.: Power loss dependence on flux change rate in tension beams

Table 3-5 Equations to calculate power loss for specific resistivity values larger than $10^{-8}\,\Omega m$

Upper tension beam	$P = 7.33*10^{-6}\sigma * n^2 = \frac{7.33*10^{-6}}{\rho} * n^2$, if n≤1
Lower tension beam	$P = 6.77*10^{-6}\sigma * n^2 = \frac{6.77*10^{-6}}{\rho} * n^2$, if n≤1

3.1.3 Tension Plates

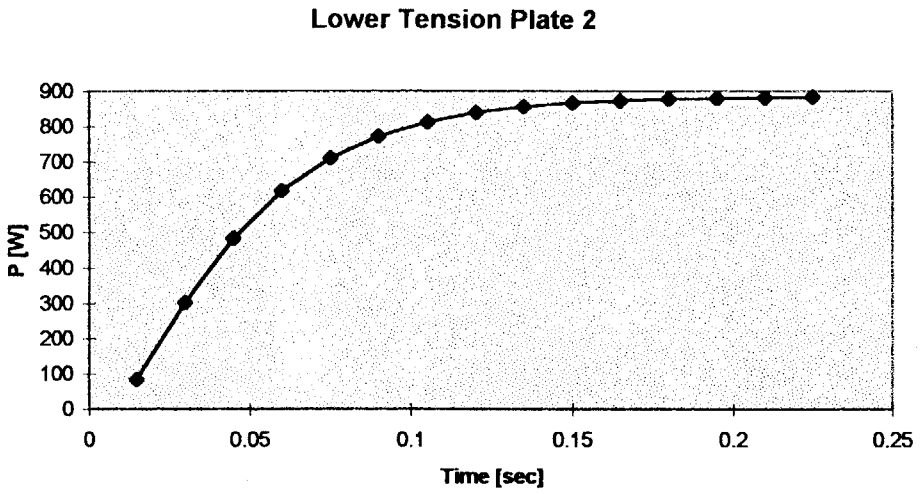

Figure 3-8.: Power loss as a function of time in lower tension plate

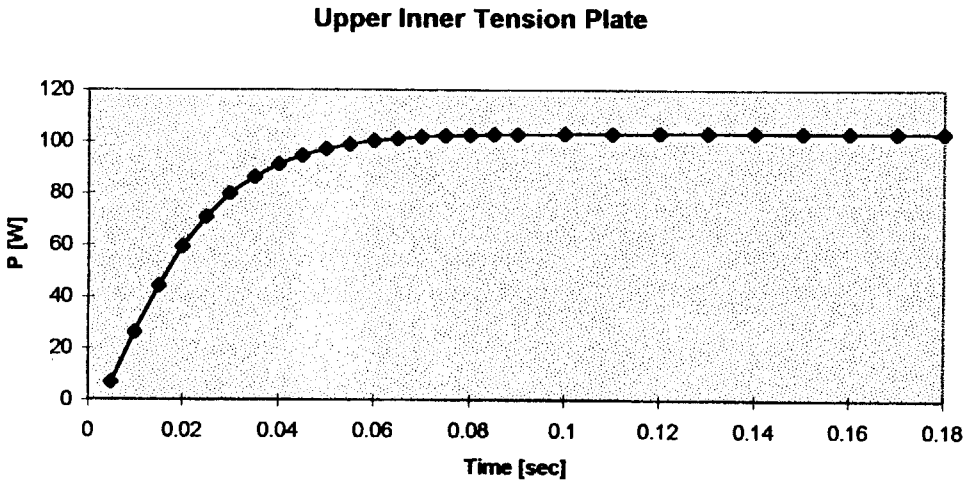

Figure 3-9

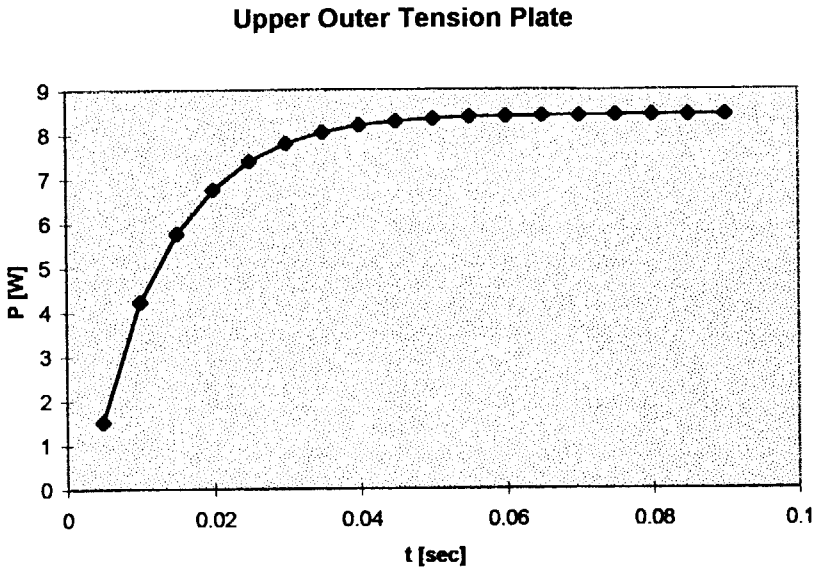

Figure 3-10

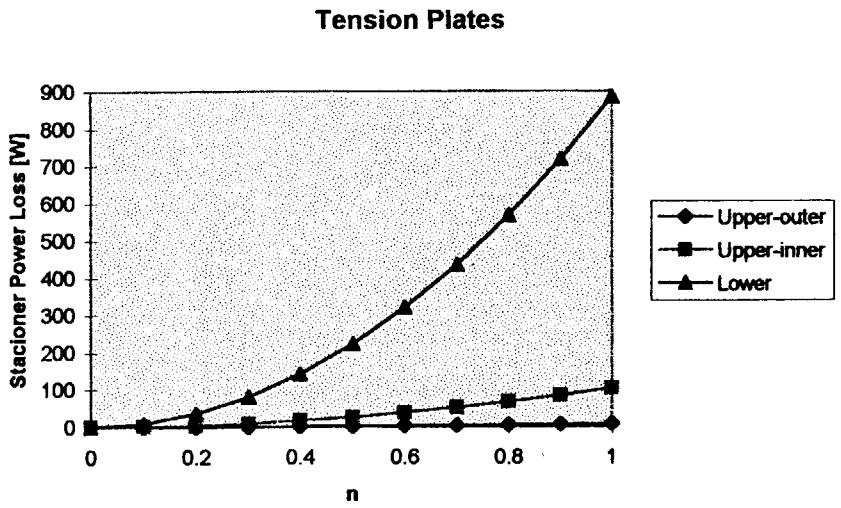

Figure 3-11.: Power loss dependence on flux change rate in tension plates

Table 3-6 Equations to calculate power loss for specific resistivity values larger than $10^{-8}\,\Omega m$

Upper, Outer Tension Plate	$P = 4.47536*10^{-6}\sigma * n^2 = \frac{4.47536*10^{-6}}{\rho} * n^2$, if n≤1
Upper, Inner Tension Plate	$P = 5.49839*10^{-5}\sigma * n^2 = \frac{5.49839*10^{-5}}{\rho} * n^2$, if n≤1
Lower Tension Plate	$P = 4.71519*10^{-4}\sigma * n^2 = \frac{4.71519*10^{-4}}{\rho} * n^2$, if n≤1

3.2 Eddy Current Loss Distribution

The absolute value of eddy current increases toward the sides of a component. Therefore the eddy current power loss is also larger near sides. As an example the power loss distribution is plotted in the cross-section of an inner tension rod, at the center in Figure 3-13. There is also a distribution in power loss due to the inhomogeneous field distribution. This is illustrated in Figure 3-12 for an inner tension rod.

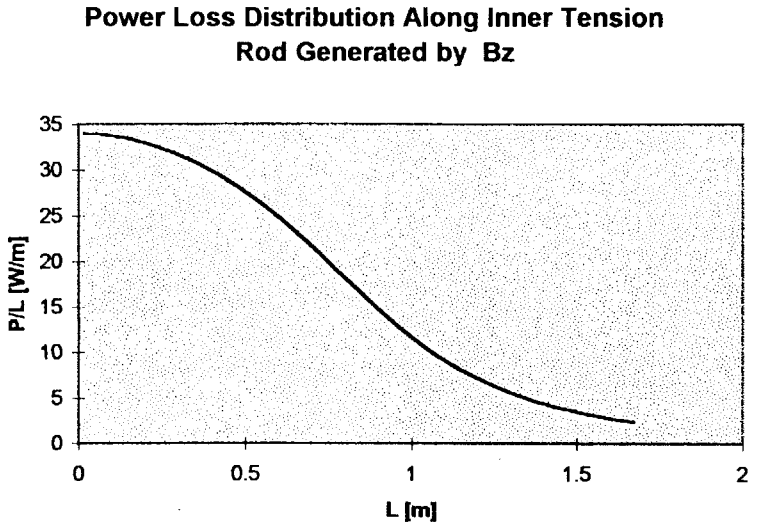

Figure 3-12

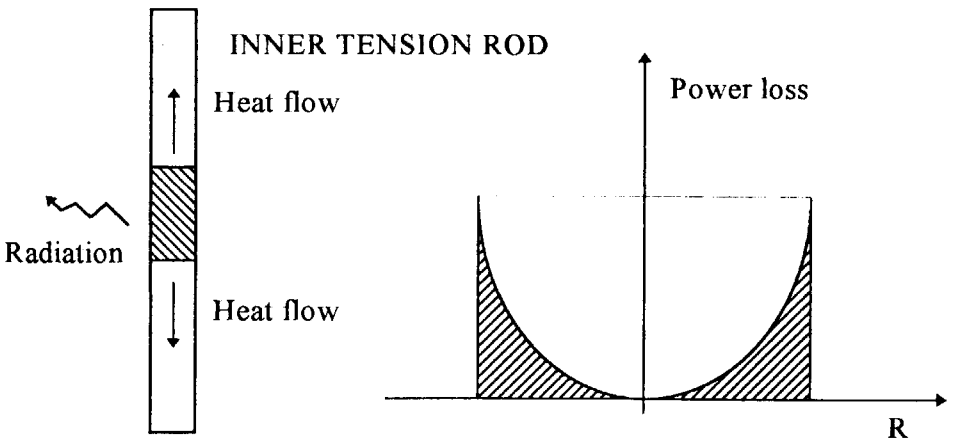

Figure 3-13.: Power loss distribution in the cross-section of an inner tension rod at its center

3.3 Eddy Currents in Connected Components

Introducing beams with plates together in the calculation the loss in beams increases a little bit while in plates decreases. Assembling the whole structure some loops can be also found. This is discussed in Section 3.5.

3.4 The Effect of BH-curve of Incoloy onto the eddy current loss

In this section not the ferromagnetic hysteresis loss is considered, but the change in eddy current loss through the change of magnetic field distribution, because of the presence of ferromagnetic material.

A 2D static nonlinear analysis is carried out with ANSYS code to obtain the flux density distribution in the cross-section of the magnet. For the nonlinear field calculation a single valued monotonically increasing BH curve was used plotted in Figure 3-14 instead of the hysteresis loop. A two-step solution sequence was applied to obtain the final solution. First an excitation ramped through five substeps was introduced, each with one equilibrium iteration. Next the final solution was calculated over one substep, with 15 equilibrium iterations.

In the case of linear model the field profile does not change with increasing excitation current, only the scale. With non-linear model outside the winding, the field is almost the same, like in linear case, however within the Incoloy winding at low excitation current it is different. A series of flux density profiles are plotted in Figure 3-15, Figure 3-16 and Figure 3-17 at different excitation current values.

Not the numeric value of the field itself determines the eddy currents but the flux change rate. We define two paths in the cross-section of the magnet. Path-1 is in the mid-plane of the winding and path-3 is in the upper plane of the winding. Figure 3-18 shows the flux density change in time in inner tension rod, where path-1 cross over it. Figure 3-19 and Figure 3-20 are plotted for path-3. Figure 3-21 Figure 3-22 and Figure 3-23 are the same for outer tension rod. At the very beginning of the excitation, the flux change rate is slightly higher in case of the ferromagnetic model, however in the main part the curves run parallel with the curves of linear model. This means, that the flux change rate is the same and hence the eddy current loss is also the same.

We can conclude, that the eddy current loss can be evaluated with the linear model in structural steel components. The flux distribution is modified by the magnetic material. However the difference in flux change rate outside the Incoloy winding is small and hence the eddy current loss is not influenced in tension rods, beams and plates.

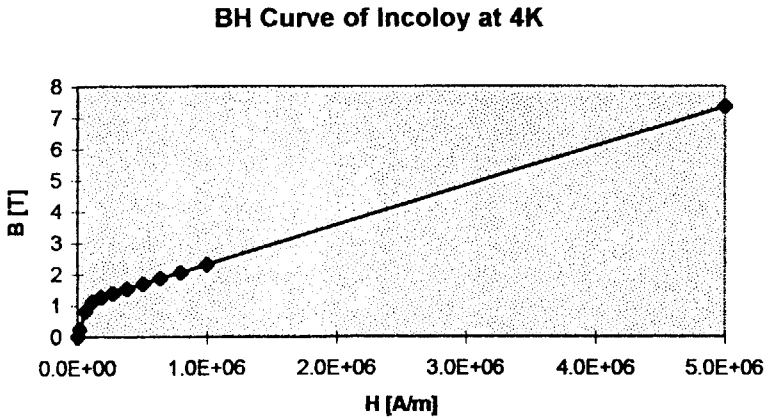

Figure 3-14.: Single valued BH curve of Incoloy applied in nonlinear numerical analysis

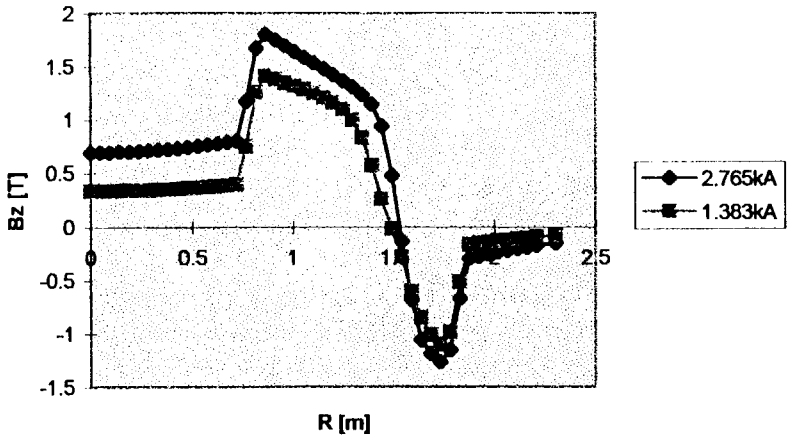

Figure 3-15.: Magnetic flux density distribution in the center of magnet in case of 1.383 kA and 2.765 kA excitation current

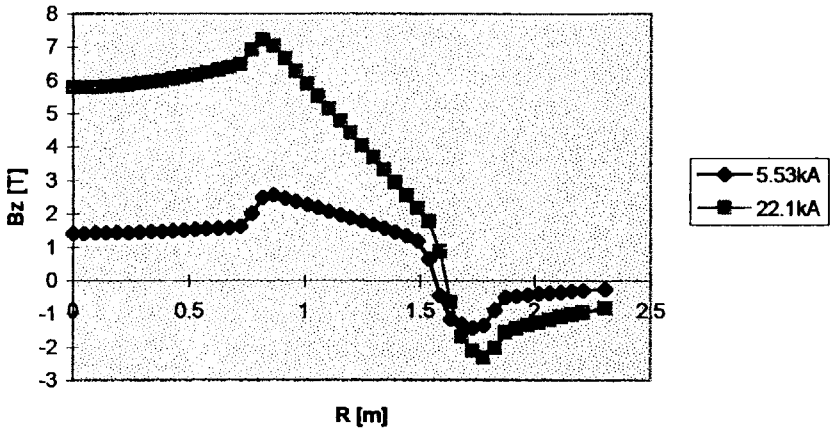

Figure 3-16.: Magnetic flux density distribution in the center of magnet in case of 5.53 kA and 22.1 kA excitation current

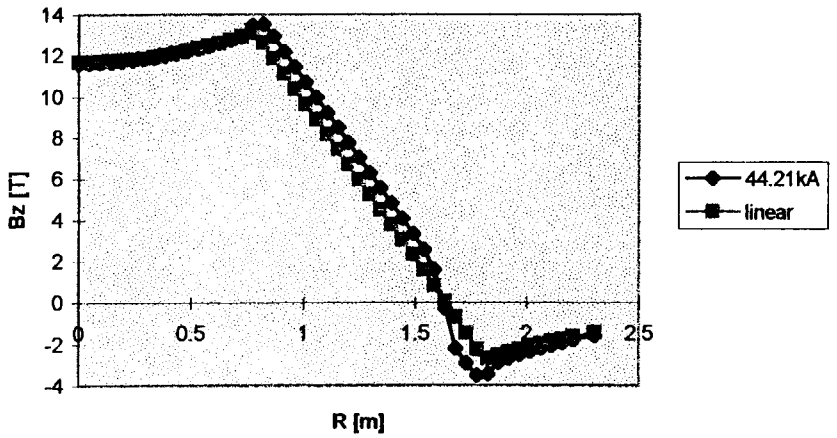

Figure 3-17.: Magnetic flux density distribution in the center of the magnet in case of 44.21 kA excitation current with linear and nonlinear material models

B vs. time in inner tension rod, path1

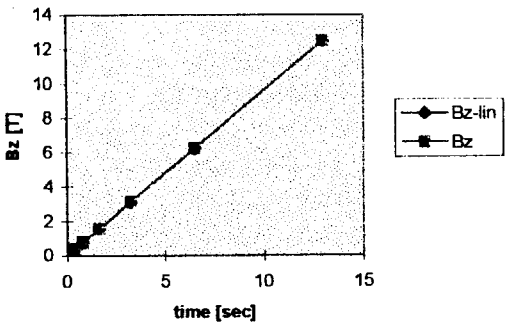

Figure 3-18

B vs. time in inner tension rod, path3

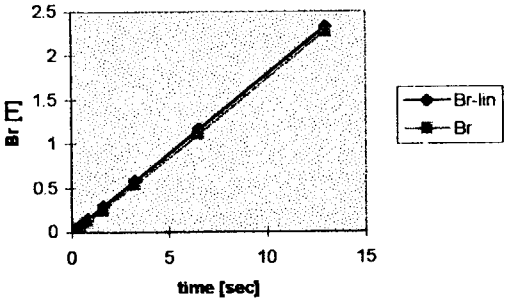

Figure 3-19

B vs. time in inner tension rod, path3

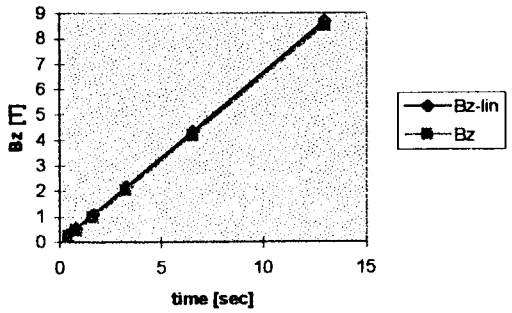

Figure 3-20

B vs. time in outer tension rod, path1

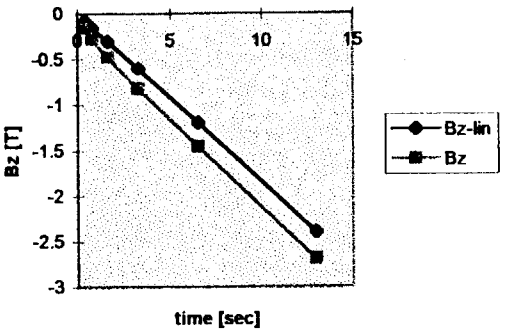

Figure 3-21

B vs. time in outer tension rod, path3

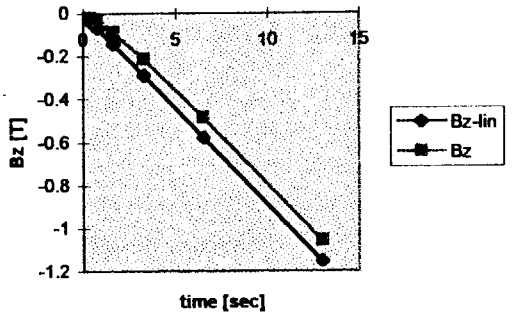

Figure 3-22

B vs. time in outer tension rod, path3

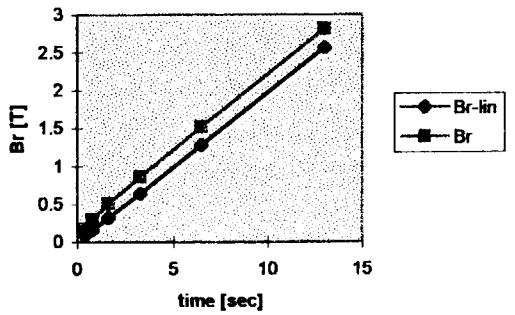

Figure 3-23

3.5 Loop Currents

3.5.1 Frame

Inner and outer tension rods together with lower and upper tension beams connected and fixed mechanically produce a frame, which is a closed loop electrically, as illustrated in Figure 3-24. If magnetic flux changing in time path through the frame, electromotive force is induced, which generates a large loop current, because of the small resistivity of the frame.

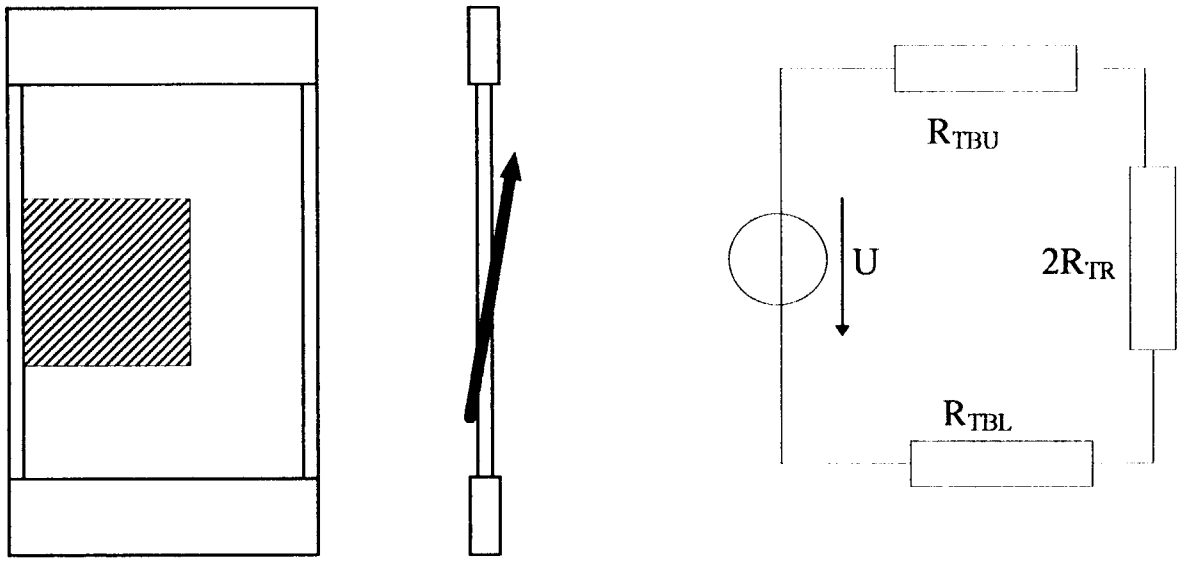

Figure 3-24.: Frame and its circuit model

To obtain the loop current (I), generated by a given EMF, the DC resistivity of tension rods (R_{TR}), upper and lower tension beams (R_{TBU} ,R_{TBL}) is estimated based on their geometry:

$$R_{DC} = \rho\frac{l}{A}$$

$$\left(\frac{l}{A}\right)_{TR} = \frac{3.376m}{0.02137m^2} = 158\frac{1}{m}$$

$$\left(\frac{l}{A}\right)_{TBU} = \frac{1.375m}{0.52*0.152m^2} = 17.396\frac{1}{m}$$

$$\left(\frac{l}{A}\right)_{TBL} = \frac{1.375m}{0.47*0.152m^2} = 19.247\frac{1}{m}$$

$$I = \frac{U}{2R_{TR} + R_{TBU} + R_{TBL}}$$

In Table 3-7 calculated resistivity values are listed, while in Figure 3-25 and Figure 3-26 loop currents and their densities are illustrated up to 0.05V electromotive force value. If loop current is present, the loop current density is superposed onto the eddy current density of tension rods and beams hence increasing the power loss. In case of ρ=5.3E-7Ωm specific resistivity and electromotive force less than 0.02V we may neglect the contribution of loop currents on the power loss.

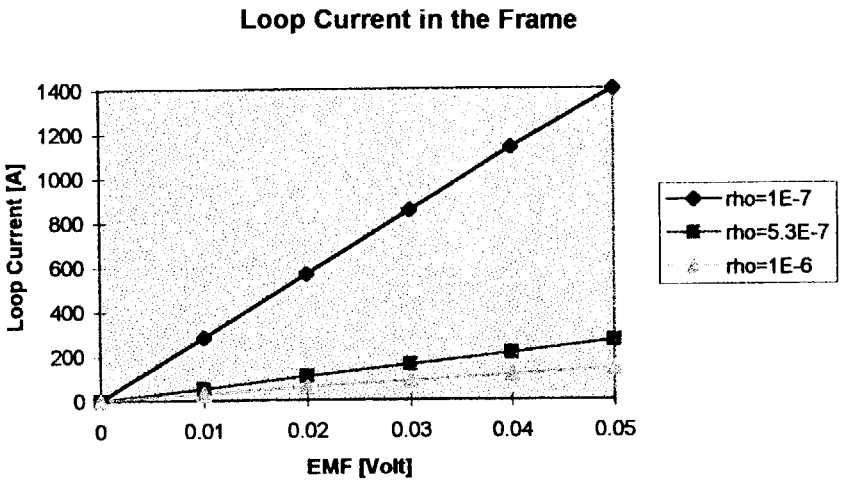

Figure 3-25.: Loop current in the frame

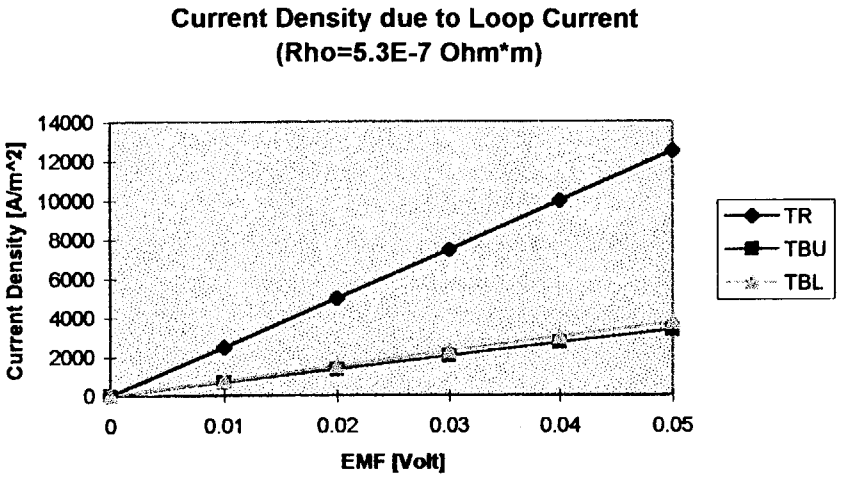

Figure 3-26.: Loop current density in frame components

Table 3-7.: Loop current in the frame

Specific Resistivity	$\rho = 1E-8\Omega m$	$\rho = 5.3279E-7\Omega m$	$\rho = 1E-6\Omega m$
Tension Rod	1.58E-6 Ohm	8.41E-5 Ohm	1.58E-4 Ohm
Upper Tension Beam	1.74E-7 Ohm	9.27E-6 Ohm	1.74E-5 Ohm
Lower Tension Beam	1.93E-7 Ohm	1.03E-5 Ohm	1.93E-5 Ohm
R	3.527E-6 Ohm	1.878E-4 Ohm	3.527E-4 Ohm
I(0.01V)	2.84 kA	53.25 A	28.4 A
I(0.02V)	5.68 kA	106.5 A	56.8 A
I(0.03V)	8.52 kA	159.8 A	85.2 A
I(0.04V)	11.36 kA	213 A	113.6 A
I(0.05V)	14 kA	266 A	140 A

In the design the flux is parallel to the frame, so no flux path through it. However in the practice small deviations may occur like:

- Misplacement of winding-pack into vertical direction
- Misplacement of winding-pack into horizontal direction
- Miss-orientation of winding-pack

First the induced EMF is roughly estimated in case when the winding-pack is miss-oriented. The maximum deviation of winding-pack from the horizontal plane is 2 mm over 3620 mm. From this the maximum angle between the plane of frame and the axis of winding-pack can be determined:

$$\sin\alpha = \frac{2}{3620}$$

Only field component perpendicular to the frame will induce loop current, which can be obtained as $B_z \sin\alpha$. An effective area is calculated with respect to the field distribution. Inside the coil and in the coil cross-section the z-component of the field is relatively large as indicated with the shaded area in Figure 3-24. Therefore we consider only this area in the flux calculation and decrease the effective area to one fourth of the original one. Moreover B_z is the largest inside and decreases linearly toward the outer region, therefore the effective area will be further decreased to half value, $A_{effective}=1/8*A_{frame}$ where $A_{frame}=4.64m^2$. Supposing 1T/sec induction change rate in the decreased effective area the induced electromotive force is obtained in the frame:

$$EMF = \frac{d}{dt}\int BdA \approx \frac{dB_z}{dt}\sin\alpha\, A_{effective} = 0.3mV .$$

3.5.2 Inter-frame loops

Frames are connected electrically with tension beams producing inter-frame loops. First only the radial component of field is considered. Permanent loops are ABCD and IJKL (connected through EH and FG).

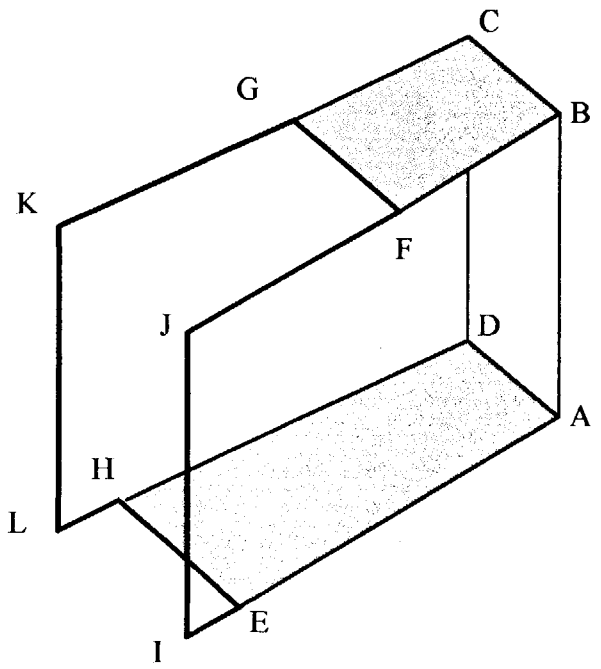

Figure 3-27.: Two frames connected with tension plates

If the winding-pack is introduced precisely, no EMF is induced in these loops, because the radial component of field opposite in sign in the upper and lower regions. However if the winding-pack is miss-placed into vertical direction, flux will path through these loops. The distances between two inner tension rods (BC) and two outer tension rods (JK) are

$$h_1 = 2R_1 \sin\alpha = 1.130 \sin\left(\frac{22.5}{2}\right) = 0.221m$$

$$h_2 = 2R_2 \sin\alpha = 3.880 \sin\left(\frac{22.5}{2}\right) = 0.757m$$

If we move the winding-pack with x and suppose 1.8T at the upper tension beam and -1.8T at the lower tension beam, than EMF_1=0.06x Volt, and EMF_2=0.21x Volt. Even if x=5cm, EMF_2=10mV.

Next the z-direction of magnetic field is considered. Every upper outer tension plate is electrically connected only to one tension beam. However upper outer plates connect two frames and lower plates connect four frames. This cause an asymmetry with respect to the induced voltage. We have to consider GFJIEHLK loop which is plotted with thick line in Figure 3-27. The area what should be considered is

$$T = \frac{1}{16}\frac{D_{OD}\pi - D_{ID}\pi}{4} = 0.28155m^2$$

The z-component of the induction in the place of upper outer tension plate is approximately 1T, hence dB/dt=1T/13sec. The induced electromotive force is EMF=22mV.

For simplicity we will neglect the contribution of loop currents during loss calculation.

3.6 Temperature increase in structural components

Before operation all components of the Model Coil is cooled down to liquid helium temperature. During the energizing process of the magnet the induced eddy currents heat up metal components. As a row estimation of temperature increase we consider one cycle of excitation which includes an increasing and a decreasing part both with duration 13 sec.
The component under examination is supposed to be insulated from its neighborhood and an infinite large heat conductivity is supposed, which is realized by a homogeneous power loss distribution. The temperature increase is evaluated by the formula

$$\int_{T_1}^{T_2} c(T)m dT = \int_{t_1}^{t_2} P dt$$

The specific heat data is summarized in Table 3-8 and plotted in Figure 3-28. The density is supposed to be $\rho_m = 7.861E3 kg/m^3$.

Table 3-8 Temperature dependence of specific heat of SS316

Temperature	Specific Heat
4K	2.206734 J kg^{-1} K^{-1}
6K	3.08733199 J kg^{-1} K^{-1}
8K	4.06794432 J kg^{-1} K^{-1}
10K	5.108969775 J kg^{-1} K^{-1}
20K	11.0069417 J kg^{-1} K^{-1}
77K	144 J kg^{-1} K^{-1}
273K	435 J kg^{-1} K^{-1}

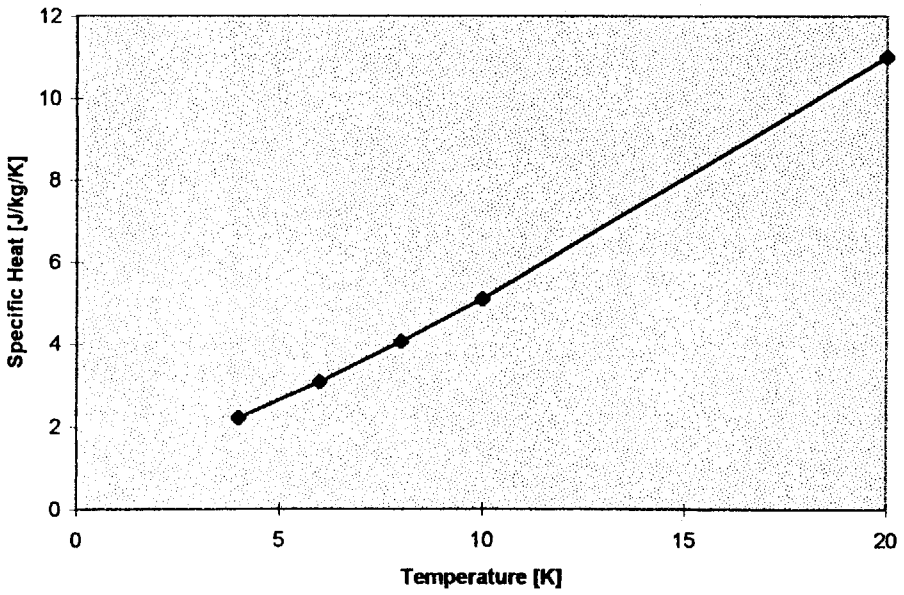

Figure 3-28 Specific heat vs. temperature of SS316

Table 3-9.: Adiabatic temperature increase estimation of structural steel components during one cycle of applied excitation (rho=5.33E-7 Ohm*m)

Component	P[W]	V[m^3]	P/V[W/m^3]	∫CdT	ΔT
Rod - Inner	60.95W	0.1m^3	610W/m^3	2.0178	0.84K
Rod - Outer	10.04W	0.1m^3	100.4W/m^3	0.3308	0.148K
Beam - Upper	13.76W	0.109m^3	126W/m^3	0.4168	0.186K
Beam - Lower	12.7W	0.098m^3	130W/m^3	0.43	0.192K
Plate - Upper, Outer	8.4W	0.03867m^3	217W/m^3	0.7178	0.316K
Plate - Upper, Inner	103.2W	0.06689m^3	1543W/m^3	5.1041	1.917K
Plate - Lower	885W	0.29146m^3	3036W/m^3	10.0428	2.341K

The results of the adiabatic temperature increase estimation is listed in Table 3-8. It can be seen, that the temperature may increase significantly due to eddy currents if the magnet is used in pulse mode for a long time. Therefore cooling is required. The largest temperature increase occurs in lower tension plates and in the in-coil part of inner tension rods where significant power loss is produced. If the specific resistivity increases due to the local increase of temperature, than a coupled heat flow and electromagnetic analysis is required which take into account the distribution of specific resistivity.

4. Loss Generated in Incoloy Jacket

4.1 Ferromagnetic Hysteresis Loss of Incoloy Jacket

In ferromagnetic materials the area of a closed minor or major loop gives the heat loss produced in unit volume and can be calculated by

$$W_{loss} = \oint HdB$$

The hysteresis loss in INCOLOY is produced at relatively low field values because of the saturation. For an exact field and loss calculation mathematical hysteresis models can be used, however this is not essential for a row estimation. As a first step it is enough to estimate the loss based on low temperature hysteresis loop measurements. At 4.2K the hysteresis loss of INCOLOY908 was found to be W_{loss}=4.4mJ/cm^3=4.4kJ/m^3 for mild annealed plus heat treated and W_{loss}=4.1mJ/cm^3=4.1kJ/m^3 for mild annealed specimens, magnetizing them on the major loop (Goldfarb 1986). If a zero averaged triangular shape wave-form is used to excite the CS Model Coil large enough to drive the total volume of Incoloy jacket into saturation, than just the total volume of Incoloy jacket used in CS1 and CS2-type conductors determine the loss.

Table 4-1 Geometric data of conductors

Location	Length	Type	Cross-section	Volume
Insert coil	144m	CS1	1440mm^2	0.20736m^3
Inner module 1-4th layer	707m	CS1	1440mm^2	1.01808m^3
Inner module 5-10th layer	1538m	CS2	996mm^2	1.53185m^3
Outer module 10-18th layer	2724m	CS2	996mm^2	2.71310m^3

Based on Table 4-1 the total volume is V=5.47m^3. This would result in 24kJ heat loss per cycle in the total amount of jacket.

4.1.1 Magnetization History

The hysteresis loss depends on the magnetization history. A trapezoidal shape excitation (in the positive plane) applied repeatedly to the CS Model Coil magnetize the Incoloy jacket only on a minor hysteresis loop.

The loss strongly depends on the shape and extreme field values of the minor loop. In present case the minimum value of field intensity produced by the excitation current is zero and the maximum value is large enough to magnetize the jacket up to saturation. Consequently one ending point of the minor loop is in saturation while the other one is located at field values between zero and -H_c depending on the location of an actual conductor. The reason why H is lowered can be explained by magnetic circuit models. If a closed magnetic circuit made of ferromagnetic material is magnetized by an external field and next the field is switched off, than we move back to the remanent induction point where H=0. However in the case of Incoloy jacket the circuit is not closed since every conductor is wrapped with a coil insulator (1.5 mm thickness) and every layer is separated with a layer insulation (3 mm thickness). From magnetic point of view this means that the ferromagnetic substance is cut into pieces by a large number of air-gaps. In this magnetic circuit the constitutive equation and the Ampere's law have to be

satisfied in the same time. This results in the strong demagnetization of Incoloy jacket and a relative increase of loss comparing to a closed magnetic loop, as illustrated in Figure 4-1.

In present row estimation the loss of minor loop is set to one third of a complete cycle 1.46mJ/cm^3 which results in 8kJ heat loss in the whole winding during a complete period of excitation.

4.1.2 Characteristic Values of Hysteresis Curves

Characteristic values of the hysteresis loop like coercive field and remanent induction also get importance in the loss calculation. Unfortunately present measurement data carried out by Goldfarb (1986) on INCOLOY 908 does not give information about details. Moreover the hysteresis loss calculated from the area of the MH-loop is not in agreement with the loss data (probably measured by calorimetric technique). One possible explanation can be, that the size of the specimen was small (0.225 cm^3) and probably very thin in order to avoid eddy current effect. However in such a case the domain structure may be different and also the number of domain walls may be too small. During magnetization the so called microscopic eddy currents can be induced in the vicinity of domain walls, due to their fast movement. These microscopic eddy currents also produce loss. They may lose their importance in a larger specimen. This should be verified by measurement.

The BH-curve measurements were carried out on mild annealed and aged specimens. However the conductor will be manufactured by a pull-down procedure followed by heat treatment. It would be important to measure BH-curve also on specimens prepared under the same condition as the jacket is produced.

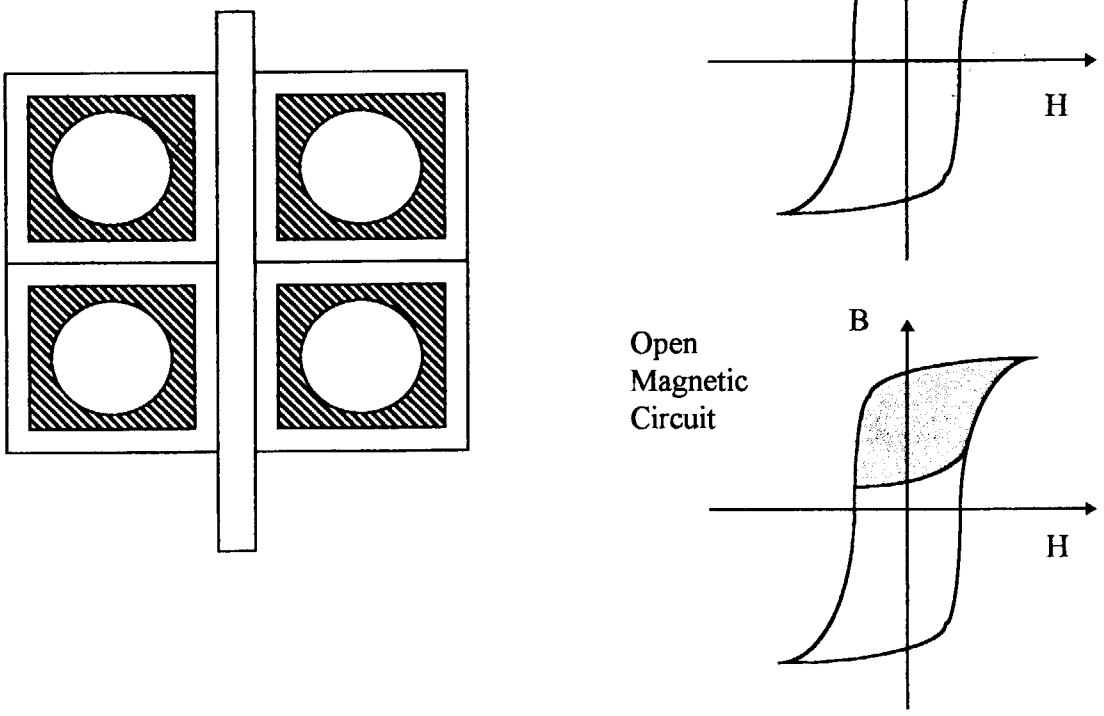

Figure 4-1

4.2 Eddy Current Power Loss of Incoloy Jacket

Assumptions and conditions for the eddy current loss analysis of Incoloy jacket:

a) The superconductor is supposed to be insulated from the Incoloy jacket. This means that no eddy currents can be closed through the superconductor, they flow in the jacket.

b) Instead of the modeling of the complicated spiral structure of the winding the conductor is cut into pieces and only one turn is considered in the same time, spanned into the horizontal plane. By summing up the contribution of individual turns, the total loss is obtained. The basis of this simplification is the following: Let us consider one turn placed into a homogeneous magnetic field slowly changing in time. The length of a turn is relatively long and by further increasing it the power loss also increases linearly with the length. The eddy currents are parallel with the coil except the end regions. In the real magnet the field is not homogeneous, but there is a gradient along the length of coil resulting in a small eddy current component, which is not parallel to the coil. Since the gradient of field is small along one turn, a good approximation of loss can be obtained by applying a piece-wise linear field distribution along the length of coil, where the field distribution is the same along one turn.

c) A simplified 2D axisymmetric model is applied to the cross-section of jacket. Only one jacket is considered in the same time for eddy current analysis and it is not excited from inside. The rest of winding is taken into account with its excitation current density and no eddy currents are considered. To satisfy the correct eddy current distribution in the cross-section of the selected jacket, the total current of jacket is forced to be zero. Since ANSYS can not apply directly the formula introduced in Part A for the current force, first an additional voltage degree of freedom was introduced to the nodes of jacket and next they were coupled. Finally the current was prescribed in one node.

d) The simplified solenoid model was used for the numerical calculation of Insert coil jackets, Inner Module-B and Outer Module jackets, while the detailed model was applied to the Inner Module-A jackets.

e) The specific resistivity was set to $\rho = 1E-8\Omega m$. The result can be recalculated for lager specific resistivity values or for smaller field rates.

f) The specific resistivity distribution is homogeneous in the jacket and does not depend on the field.

g) Only half of the magnet is considered because of the symmetry.

For our convenience the layers are numbered as follows; Inner Module-A 1-4, Inner Module-B 1-6, Outer Module 1-8. Conductors are also numbered starting from the center of the magnet.

As the magnet is energized eddy currents are built up through a short time transient. In Figure 4-2 the eddy current power loss is plotted in time generated in Insert Coil conductor Number 2. Following the transient, in stationer state the power loss does not change anymore if the resistance also does not change. (In case of temperature increase or due to magneto-resistance effect the resistance may increase.)

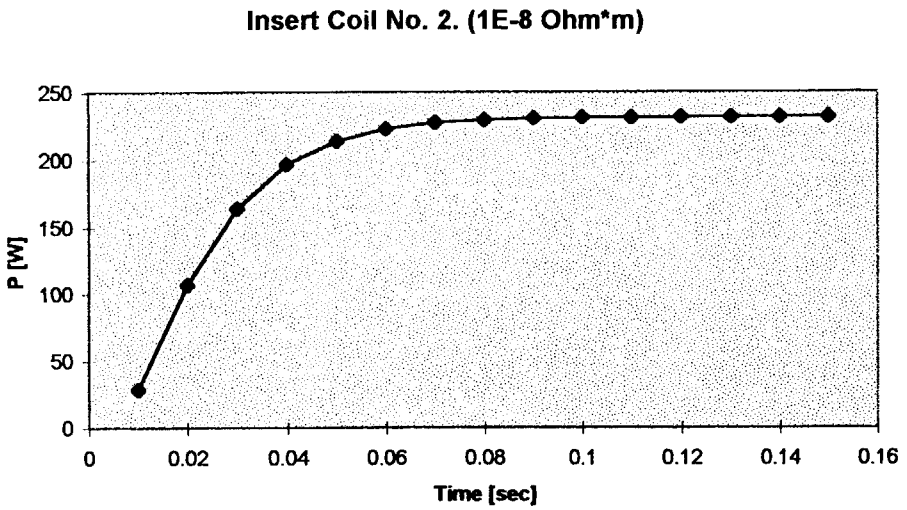

Figure 4-2.: Eddy Current Power Loss vs. Time in Insert Coil Jacket No.2

The individual turns are subjected to different fields depending on their location. Not only the amplitude of flux density is changing but its incidence angle as well. Therefore several conductor were analyzed in every layer. The results are plotted in Figure 4-3 for Insert Coil, in Figure 4-4 and Figure 4-6 for Inner Module A and B and in Figure 4-8 for Outer Module. The power loss values are also plotted along the radius in Figure 4-5, Figure 4-7, and Figure 4-9. The power loss for the rest of conductors are interpolated and the total power loss is obtained by summation and listed in Table 4-2, Table 4-3, Table 4-4, and Table 4-5.

4.2.1 Insert Coil

Table 4-2.: Stationer Eddy Current Power Loss in Insert Coil Incoloy Jacket (CS1-type conductor, $\rho = 10^{-8}\Omega m$, $dI/dt = 46kA/13\sec$, simplified model)

Conductor	P [W]
No.2	232W
No.5	224W
No.10	195W
No.15	143W
Total in Insert Coil	6000W

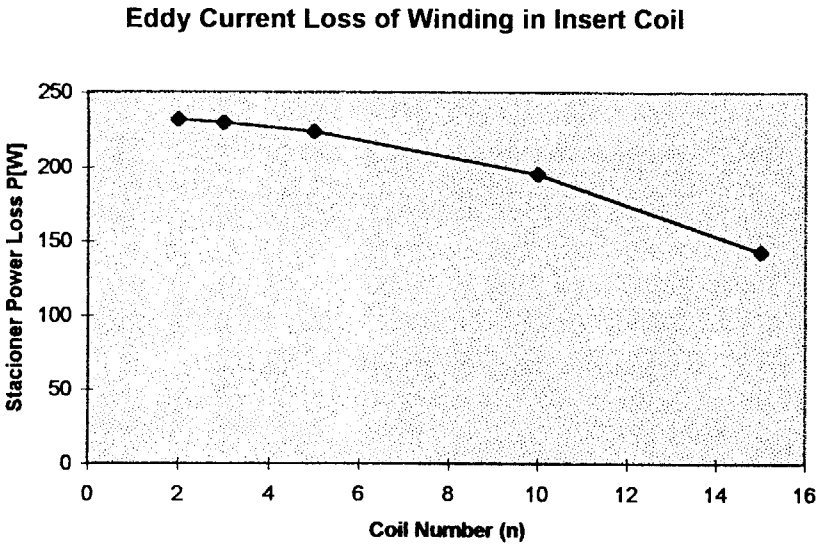

Figure 4-3

4.2.2 Inner Module-A

Table 4-3.: Stationer Eddy Current Power Loss in Inner Module-A Incoloy Jacket (CS1-type conductor, $\rho = 10^{-8}\,\Omega m$, $dI/dt = 46kA/13\,\mathrm{sec}$, detailed model)

Conductor	Layer-1	Layer-2	Layer-3	Layer-4
No.2	219.83W	205.85W	190.60W	174.4W
No.5	212.65W	199.42W	185.06W	169.84W
No.10.	184.06W	174.11W	163.84W	153.08W
No.15	134.77W	134.89W	134.92W	134.57W
Total in Layer	5672W	5385W	5075W	4745W
Total in Inner Module-A	20877W			

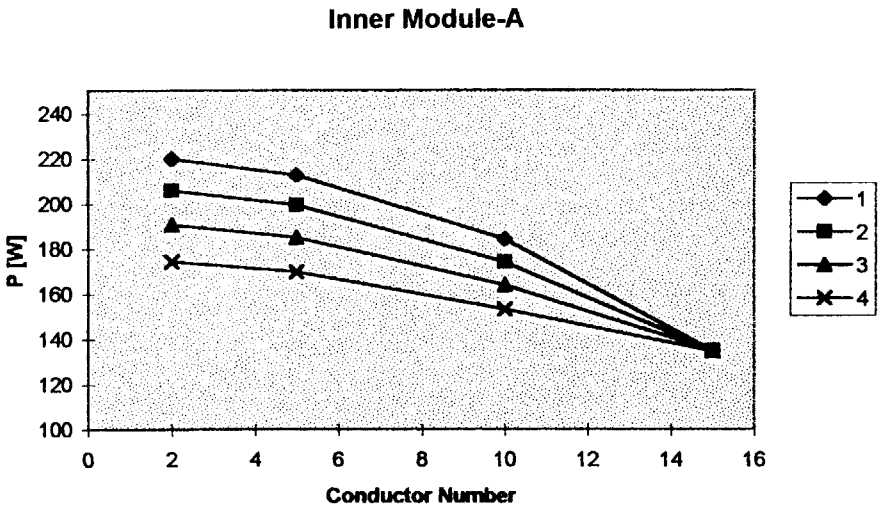

Figure 4-4

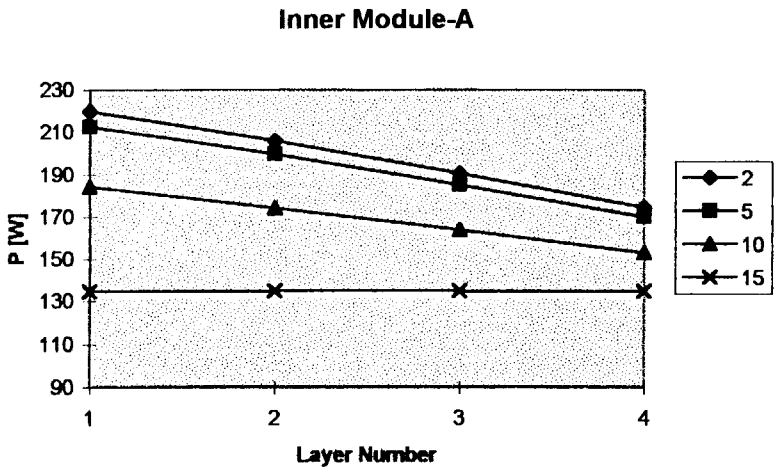

Figure 4-5

4.2.3 Inner Module-B

Table 4-4.: Stationer Eddy Current Power Loss in Inner Modul-B Incoloy Jacket (CS2-type conductor, $\rho = 10^{-8}\Omega m$, $dI/dt = 46kA/13\sec$, simplified model)

Conductor	Layer-1	Layer-2	Layer-3	Layer-4	Layer-5	Layer-6
No.2	88.48W		65.63W			34.16W
No.5	86.95W		64.99W			34.67W
No.10	81.30W		63.06W			37.57W
No.15	74.47W		63.54W			47.16W
Total in Layer	2780W	2488W	2169W	3536W		1340W
Total in Inner Module-B	12340W					

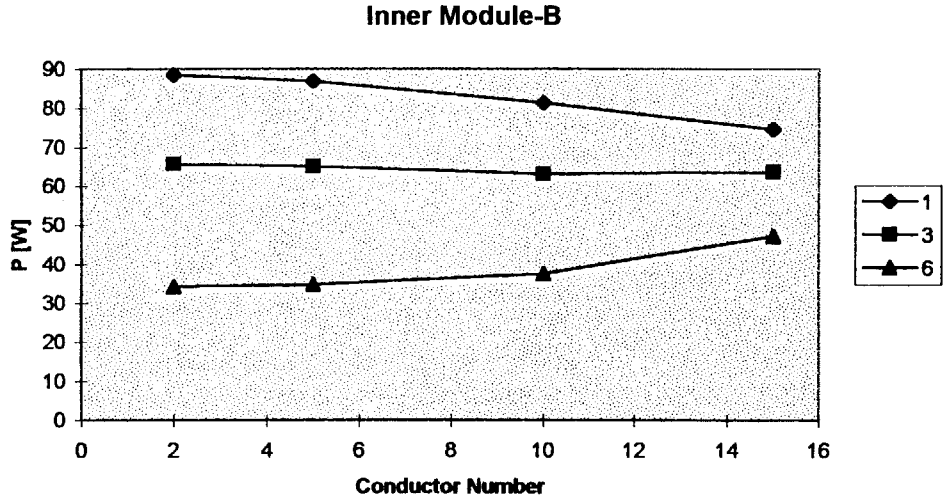

Figure 4-6

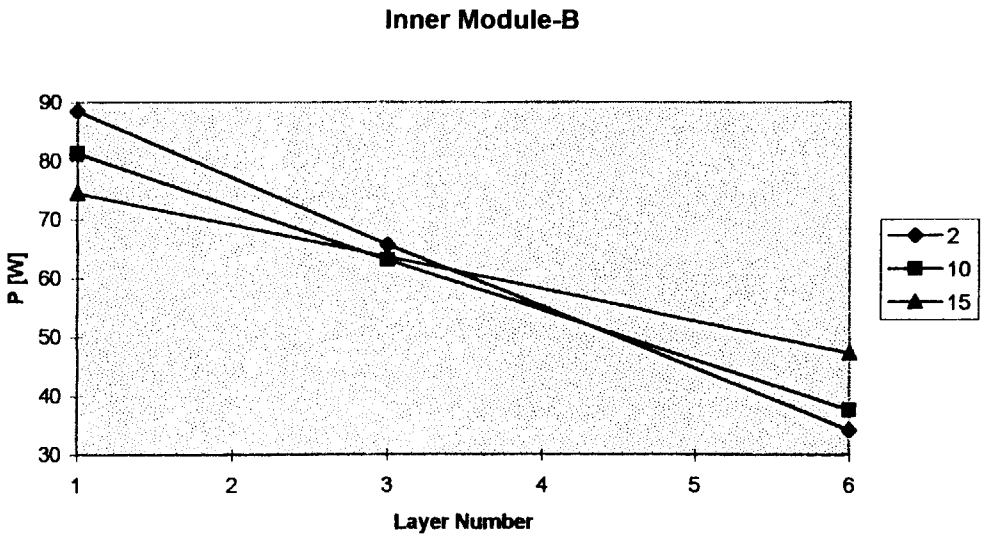

Figure 4-7

4.2.4 Outer Module

Table 4-5.: Stationer Eddy Current Power Loss in Outer Module Incoloy Jacket
(CS2-type conductor, $\rho = 10^{-8}\Omega m$, $dI/dt = 46kA/13\sec$, simplified model)

	Layer-1	Layer-2	Layer-3	Layer-4	Layer-5	Layer-6	Layer-7	Layer-8
Con. 2	19.44		6.6W		0.39W		2.9W	8.16W
Con. 5	20.43		7.9W		1.71W		3.96W	9.0W
Con. 10	25.25		13.94W		7.69W		8.64W	12.64W
Con. 15	38.41		29.26W		22.34W		19.41W	20.41W
In layer	942W	750W	557W	442W	327W	334W	340W	458W
In Outer Module	4150W							

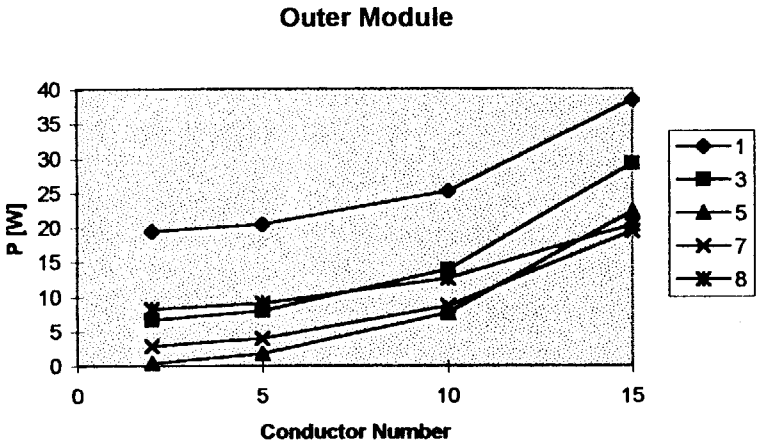

Figure 4-8

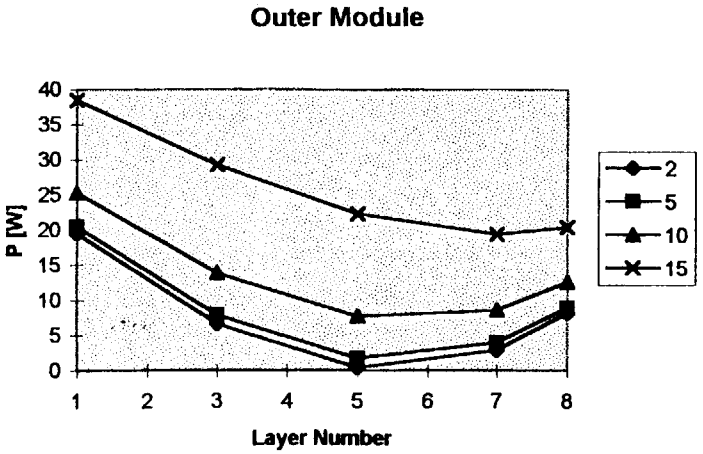

Figure 4-9

4.3 Eddy Current Power Loss Dependence on Specific Resistivity and Flux Change Rate

Table 4-6.: Formulas for the calculation of eddy current power loss in modules

Insert Coil	$P = 6*10^{-5}\sigma*n^2 = \frac{6*10^{-5}}{\rho}*n^2$
Inner Module-A	$P = 2.0877*10^{-4}\sigma*n^2 = \frac{2.0877*10^{-4}}{\rho}*n^2$
Inner Module-B	$P = 1.234*10^{-4}\sigma*n^2 = \frac{1.234*10^{-4}}{\rho}*n^2$
Outer Module	$P = 4.15*10^{-5}\sigma*n^2 = \frac{4.15*10^{-5}}{\rho}*n^2$

In Table 4-6 analytical formulas are listed for the loss calculation in different modules as a function of current change rate and specific resistivity. In addition the power loss may also decrease with increasing field if magneto-resistance effect is significant (Figure 4-10).

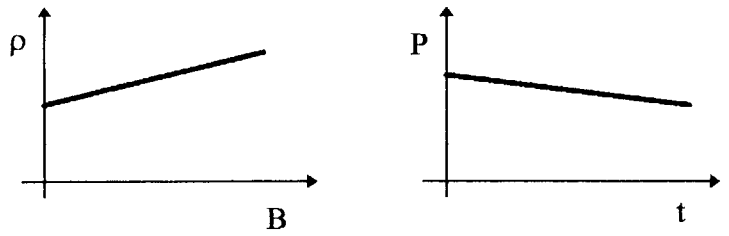

Figure 4-10.: Power loss decrease due to magneto-resistance effect

4.4 Eddy Current Power Loss Distribution in the Winding

The distribution of stationer eddy current power loss generated in layers is illustrated in Figure 4-11. Now the numbering starts at Inner Module-A, layer-1 and increases toward the Outer Module layers. A sharp drop in power loss can be observed between layer 4, where CS1-type conductor is used, and layer-5, where CS2-type conductor is applied, since the size of CS2-type conductor is smaller than that of CS1.

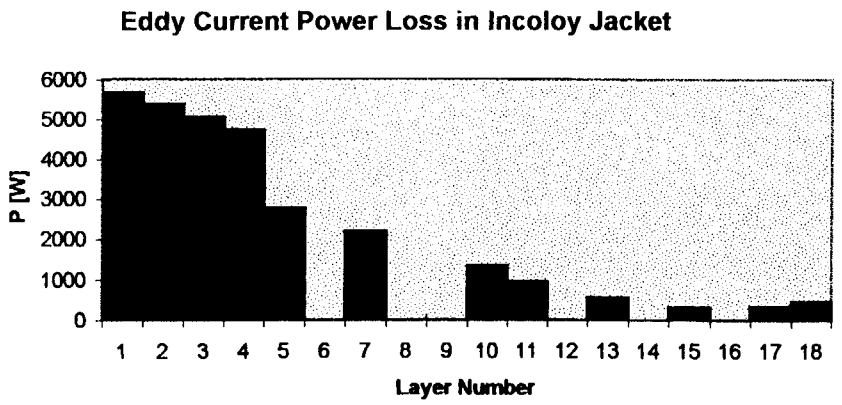

Figure 4-11.: Eddy current power loss distribution within layers

4.5 The Effect of BH-curve of Incoloy onto the Eddy Current loss of Jacket

Similarly to Section 3.4 the flux change rate is studied within the Incoloy jacket, see Figure 4-12 and Figure 4-13. At the very beginning of the excitation, the flux change rate is significantly higher than in linear case resulting in an increased eddy current loss. However over saturation it is the same as in linear case. Due to the small duration of the increased part we may neglect the difference and apply a linear model for loss calculation.

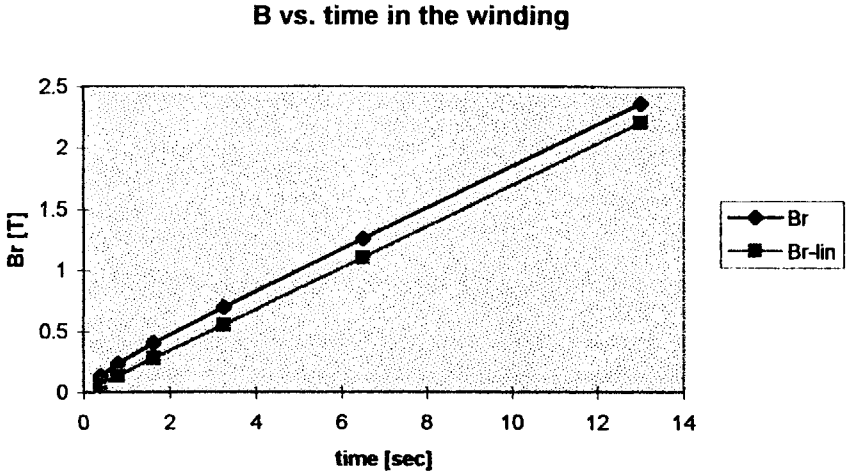

Figure 4-12.: Flux density change in time inside the Incoloy winding during the energizing of magnet

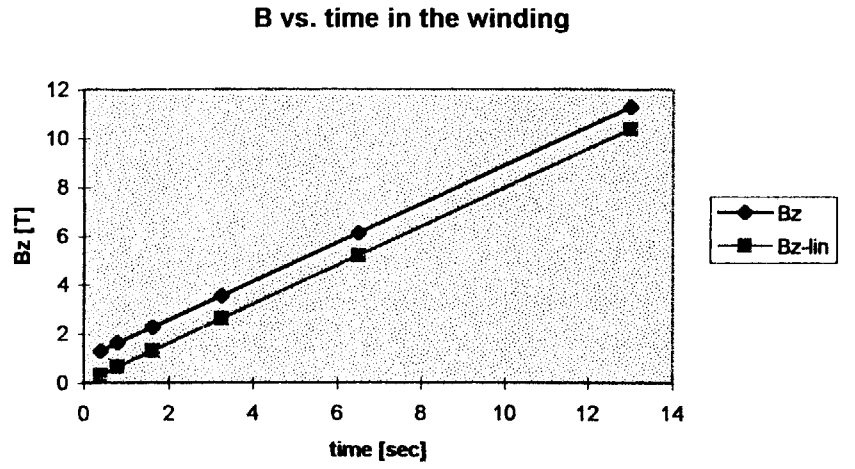

Figure 4-13.: Flux density change in time inside the Incoloy winding during the energizing of magnet

5. AC Loss of Superconducting Cables

We assume that AC losses consist only of hysteresis loss and coupling loss. The characteristic parameters of superconducting cables are summarized in Table 5-1.

Table 5-1.: Characteristic parameters of strands and filaments

Number of strands in CS1-type cables	1152 Nb_3Sn twisted filamentary composit
Number of strands in CS2-type cables	720 Nb_3Sn strand and 360Cu wire
Composite diameter	d=0.81mm
Number of filaments	N=8037
Filament diameter	2a=2.8μm
Critical current density (for transport current)	J_c(B=12T)=580A/mm^2=5.8 10^{8}A/m^2
Hysteresis loss for cyclic field	W_{loss}(B_m=+-3T)= 110mJ/cm^3
Cu/non Cu ratio in strand	1.5

5.1 Superconducting hysteresis loss in Nb_3Sn filaments

Type-II superconductor, Nb_3Sn is used in CS Model coil which exhibit magnetic hysteresis caused by the pinning of the filaments by lattice defects. The amplitude of the field which just penetrates to the center of the sample is small

$$B_p = {2\mu_0 J_c 2a}/{\pi} =< 0.1T$$

comparing to the applied transverse field,

$$\beta = \frac{B_m}{B_p} > 100,$$

therefor the energy loss per unit volume over the full penetration can be evaluated by

$$Q = \frac{B_m^2}{2\mu_0}\frac{4}{3\beta} = \frac{8}{3\pi} J_c a B_m .$$

The energy loss generated below full penetration

$$Q_p = 0.623\frac{B_p^2}{2\mu_0} < 2.5 {kJ}/{m^3},$$

will be neglected. However we have to take into consideration the dependence of critical current density on the actual magnetic field and evaluate the loss by the formula

$$Q = \frac{8}{3\pi} a \int_0^{B_m} J_c(B) dB .$$

If one knows the critical current density dependence as a function of magnetic field, can calculate the superconducting hysteresis loss. Not the critical current density given in Table 5-1 will be used, but the measured hysteresis loss data. The modified Yasukochi-model is used in order to take into consideration the critical current density dependence on the magnetic field

$$J_c(B) = \frac{J_{cb}}{\sqrt{|B|}}\left(1 - \frac{|B|}{B_{c2}}\right)^2$$

where B_{c2}=23.5T will be used considering T=4.2K temperature and ε=-0.25% longitudinal strain. After integration

$$Q = \frac{8}{3\pi} a J_{cb} \int_0^{B_m} \frac{1}{\sqrt{B}} \left(1 - \frac{B}{23.5}\right)^2 dB = \frac{8}{3\pi} 2a J_{cb} \left[B^{\frac{1}{2}} - \frac{2}{23.5}\frac{1}{3} B^{\frac{3}{2}} + \frac{1}{23.5^2}\frac{1}{5} B^{\frac{5}{2}} \right]_0^{B_m}$$

J_{cb} can be determined from the measurement result of a single filament placed in transverse magnetic field and next can be used to evaluate the superconducting hysteresis loss in the CS Model Coil. Since filament diameter may strongly scatter in a strand, for loss calculation a new constant, C is introduced which includes all of the unknown parameters

$$C = \frac{8}{3\pi} 2a J_{cb} .$$

5.1.1 Single Nb_3Sn strand in cyclic transverse magnetic field

To determine the quality of Nb_3Sn strands, the loss was measured in the case of fully reversed cyclic excitation with 3T amplitude. The hysteresis loss was found to be 110mJ/cm^3 projected to the non-copper volume. From this

$C=69.182*10^3$ and

$J_{cb}=2.91*10^{10}AT^{1/2}/m^2$.

As an example the critical current densities at 5T and 12T are the following

$J_c(5T)=8*10^9A/m^2$

$J_c(12T)=2*10^9A/m^2$.

5.1.2 Superconducting Hysteresis Loss in the CS Model Coil

The coupling between filaments and also between strands will be neglected during the hysteresis loss calculation. Moreover the loss in case of trapezoidal shape excitation is supposed to be half of fully transverse cyclic field. Also the effect of transport current is neglected. The total loss coming from the superconducting hysteresis is obtained by summing up the loss for all of the filaments:

$$W = \sum_i Q_i V_i = \frac{1}{2} \sum_i C \left[B_{m,i}^{\frac{1}{2}} - \frac{2}{23.5}\frac{1}{3} B_{m,i}^{\frac{3}{2}} + \frac{1}{23.5^2}\frac{1}{5} B_{m,i}^{\frac{5}{2}} \right] 2 r_i \pi A \qquad \left[J/cycle \right].$$

where the total non-copper areas of strands are

$A=1152A_{strand}/2.5=237.45*10^{-6}$ m^2 for CS1-type cable and

$A=720A_{strand}/2.5=148.4*10^{-6}$ m^2 for CS2-type cable.

($A_{strand}=0.81^2\pi/4=0.515299735mm^2$).

Table 5-2.: Superconducting Hysteresis Loss in CS Model Coil
(the effect of transport current is not included)

	With Insert Coil		Without Insert Coil	
	P[kW] (26sec)	Q[kJ/cycle]	P[kW] (26sec)	Q[kJ/cycle]
Insert Coil	0.11kW	2.87kJ	0	0
Inner Module-A	0.51kW	13.26kJ	0.51kW	13.28kJ
Inner Module-B	0.64kW	16.66kJ	0.64kW	16.68kJ
Outer Module	0.83kW	21.44kJ	0.82kW	21.40kJ
Total	2.09kW	54.22kJ	1.98kW	51.36kJ

5.2 Coupling Loss

Let t_m denote the ramp-up time and τ the decay time constant of coupling currents. In present application t_m is set to 13 sec and τ is supposed to be 50 msec both for CS1 and CS2-type conductor including Cu-wires. Since t_m is large comparing to τ, the coupling power loss density can be written as

$$\frac{P_{cp}}{V} = \frac{2}{\mu_0}\left(\frac{B_m}{t_m}\right)^2 \tau = \frac{2}{4\pi 10^{-7}} \frac{B_m^2}{50^2} 13 * 10^{-3} = 470.873 B_m^2 \quad \left[\frac{W}{m^3}\right].$$

The energy loss density for a complete cycle is

$$\frac{Q_{cp}}{V} = 2\frac{P_{cp}}{V} t_m = 12.243 B_m^2 \quad \left[\frac{kJ}{m^3 cycle}\right].$$

Next we have to sum up the contribution of conductors in CS Model Coil depending on their geometric positions;

$$P = \sum_i \left(\frac{P}{V}\right)_i 2 r_i \pi A$$

$$Q = 2 P t_m$$

where

A=1152A_{strand}=593.625mm^2 for CS1-type cable and
A=(360+720)A_{strand}=556.524mm^2 for CS2-type cable.
(A_{strand}=0.81$^2\pi$/4=0.515299735mm^2).

Table 5-3.: Coupling loss in CS Model Coil

n=1, τ=50msec	With Insert Coil		Without Insert Coil	
	P[kW]	Q[kJ/cycle]	P[kW]	Q[kJ/cycle]
Insert Coil	6.16kW	160kJ	0	0
Inner Module-A	21.55kW	560kJ	21.95kW	570kJ
Inner Module-B	20.36kW	529kJ	20.54kW	534kJ
Outer Module	8.24kW	214kJ	8.17kW	212kJ
Total	56.31kW	1464kJ	50.67kW	1317kJ

The results can be recalculated for other time constant or ramp up time with the following formulas:

$$P(n,\tau) = \frac{n^2 \tau}{50 m\sec} P(n=1, \tau = 50 m\sec),$$

$$Q(n,\tau) = \frac{n\tau}{50 m\sec} Q(n=1, \tau = 50 m\sec).$$

Measurements were carried out on a short piece of CS2-type conductor by K. Matsui et. al. [3]. The estimated time constant was found to be τ=13 msec including Cu-wires. Time constant of CS1-type conductor is probably larger because it contains only superconducting strands.

6. Loss of Joints

Two types of joints are applied in CS Model Coil, a Lap-type one and a Butt-type one. In Insert Coil and Inner Module only Lap-type joints are used, while in Outer Module Butt-type joints except the terminal joints which are Lap-type. In Inner and Outer Modules two conductors are winded parallel while in Insert Coil only one conductor is used. The number of conductors are (2n-1)+2 and n+1 in modules and Insert Coil respectively, where n denotes the number of layers.

The loss has two origins. One part is AC loss due to the changing magnetic field, and the other part is caused by the large transport current. The following characteristic parameters will be used for loss calculation after the measurement and estimation of Superconducting Magnet Laboratory, (see also [4]);

- AC Loss of Lap-type joint is 73W if dB/dt=0.4T/sec
- Resistivity of Lap-type joint is 6.4nΩ at 46kA and B=4.5T
- AC Loss of Butt-type joint is 6.7W if dB/dt=0.4T/sec
- Resistivity of Butt-type joint is 3.7nΩ at 46kA and B=4.5T

Different joints are located at different geometric locations above and below the upper and lower tension plates and affected by different fields. In this simple estimation this will not be considered. 0.2T/sec flux density change rate is supposed in outer module joints and 0.4T/sec in inner module joints. The field dependence of contact resistivity will be also neglected.

In Table 6-1 the numerical values of power loss are summarized. The loss increase is parabolic due to transport current up to t_1=13 sec, since the feeding current increases linearly;

$P(0<t<t_1)=P_{AC}+P_{t\ max}*(t/13)^2$.

Over t_1 up to t_2 the feeding current is constant (46kA) so no AC loss component is present;

$P(t_1<t<t_2)=P_{t\ max}$.

And finally between t_2 and t_3 in the case of decreasing field the loss behaves similarly to increasing case;

$P(t_2<t<t_3)=P_{AC}+P_{t\ max}*(t_3-t)^2/13^2$.

Table 6-1.: Loss of Joints in CS Model Coil

	Type of Joints	AC Loss of Joints, P_{AC}	$P_{t\ max}$ due to transport current (I=46kA)
Insert Coil	Lap-type 2	146W	20W
Inner Module	Lap-type 21	1533W	284W
Outer Module	Lap-type 2 Butt-type 15	37W 25W	27W 117W
Total with Insert Coil Total without Insert Coil		1741W 1595W	448W 428W

For other flux change rates the loss can be recalculated with the following formulas:

$P_{AC}(n)=P_{AC}(n=1)*n^2$

$P_{t\ max}(n)=P_{t\ max}(n=1)*n$.

The eddy currents caused by the changing magnetic field and the transport current are present in the same time, therefore their interaction should be also considered. The loss due to transport current and eddy current can not be simple superposed. Unfortunately this interaction cause further increase in the loss.

7. Summary of Loss Calculation

7.1 Eddy Current Power Loss of Structural Elements

Table 7-1 Power loss in case of $\rho = 5.3279*10^{-7}\,\Omega m$ specific resistivity and electrically insulated metal components

Component	One piece	Number of pieces	Total with Insert Coil	Total Without Insert Coil
Tension Rod - Inner	60.95W	16	975.2W	861W
Tension Rod - Outer	10.04W	16	160.6W	141.8W
Tension Beam - Upper	13.76W	16	220.2W	194.4W
Tension Beam - Lower	12.7W	16	203.2W	179.4W
Tension Plate - Upper, Outer	8.4W	16	134.4W	118.7W
Tension Plate - Upper, Inner	103.2W	8	825.6W	728.9W
Tension Plate - Lower	885W	4	3540W	3125.3W
Total structural steels			6059W	5349W

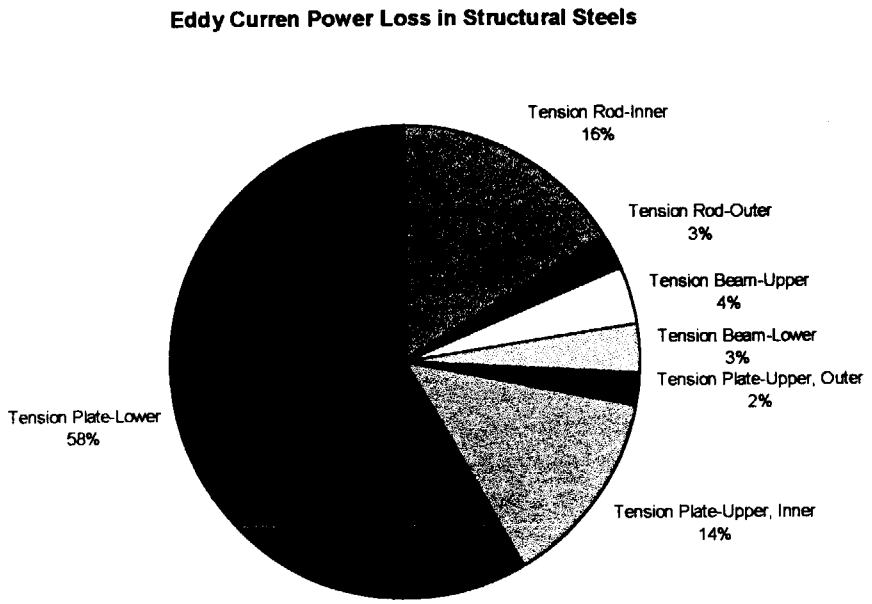

7.2 Loss of Incoloy Jacket

7.2.1 Eddy Current Loss of Incoloy Jackets

	With Insert Coil	Without Insert Coil
Insert Coil	120W	
Inner Module/A	418W	369W
Inner Module/B	246W	217W
Outer Module	83W	73W
Total in jackets	868W	766W

Specific resistivity is supposed to be $\rho = 5E-7\Omega m$.

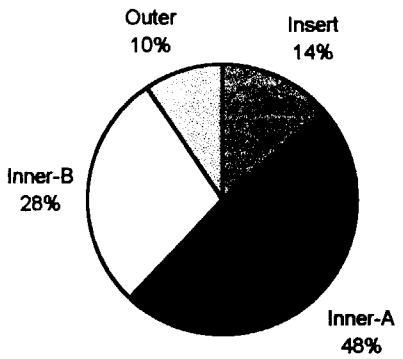

Figure 7-1

7.2.2 Hysteresis Loss of Incoloy Jackets

8kJ/cycle; independent of excitation frequency. It is produced at the beginning and at the end of excitation cycle.

7.3 AC Loss of Superconducting cable

7.3.1 Superconducting Hysteresis Loss

	With Insert Coil		Without Insert Coil	
	P[kW] (26sec)	Q[kJ/cycle]	P[kW] (26sec)	Q[kJ/cycle]
Insert Coil	0.11kW	2.87kJ	0	0
Inner Module-A	0.51kW	13.26kJ	0.51kW	13.28kJ
Inner Module-B	0.64kW	16.66kJ	0.64kW	16.68kJ
Outer Module	0.83kW	21.44kJ	0.82kW	21.40kJ
Total	2.09kW	54.22kJ	1.98kW	51.36kJ

Superconducting Hysteresis Loss

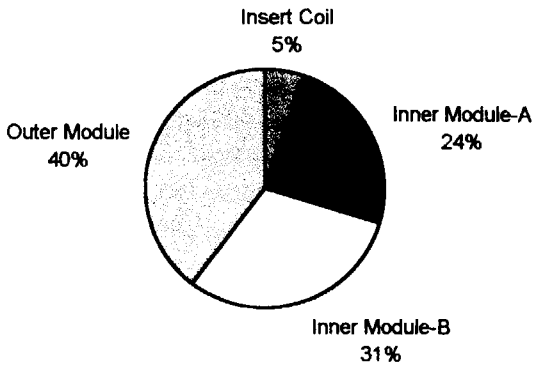

7.3.2 Coupling Loss

n=1, τ=50msec	With Insert Coil		Without Insert Coil	
	P[kW]	Q[kJ/cycle]	P[kW]	Q[kJ/cycle]
Insert Coil	6.16kW	160kJ	0	0
Inner Module-A	21.55kW	560kJ	21.95kW	570kJ
Inner Module-B	20.36kW	529kJ	20.54kW	534kJ
Outer Module	8.24kW	214kJ	8.17kW	212kJ
Total	56kW	1464kJ	50.67kW	1317kJ

Coupling Loss

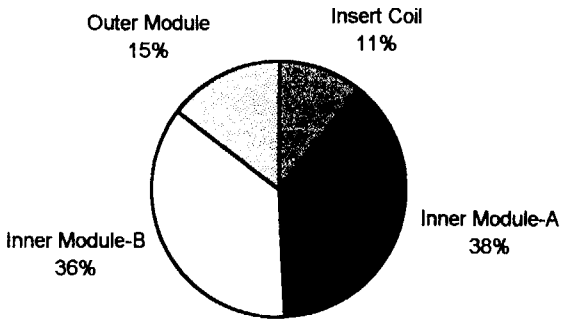

7.4 Loss of Joints

Insert Coil	$146+20*(t/13)^2$ [W] 20W $146+20*(t_3-t)^2/13^2$ [W]	if $0<t<t_1$ if $t_1<t<t_2$ if $t_2<t<t_3$	P_{AVG}=153W
Inner Module	$1533+284*(t/13)^2$ [W] 284W $1533+284*(t_3-t)^2/13^2$ [W]	if $0<t<t_1$ if $t_1<t<t_2$ if $t_2<t<t_3$	P_{AVG}=1628W
Outer Module	$62+144*(t/13)^2$ [W] 144W $62+144*(t_3-t)^2/13^2$ [W]	if $0<t<t_1$ if $t_1<t<t_2$ if $t_2<t<t_3$	P_{AVG}=110W
Total with Insert Coil	$1741+448*(t/13)^2$ [W] 448W $1741+448*(t_3-t)^2/13^2$ [W]	if $0<t<t_1$ if $t_1<t<t_2$ if $t_2<t<t_3$	P_{AVG}=1890W
Total without Insert Coil	$1595+428*(t/13)^2$ [W] 428W $1595+428*(t_3-t)^2/13^2$ [W]	if $0<t<t_1$ if $t_1<t<t_2$ if $t_2<t<t_3$	P_{AVG}=1738W

Table 7-2.: Power Loss of Joints

7.5 Total Power Loss

46kA/13sec (n=1)	With Insert Coil	Without Insert Coil
Eddy Current Power Loss of Structural Steel Components	6059W	5349W
Eddy Current Loss of Incoloy Jacket	868W	766W
Ferromagnetic Hysteresis Loss of Incoloy Jacket	308W (8kJ/cycle)	300W (8kJ/cycle)
Superconducting Hysteresis Loss	2090W (54.22kJ/cycle)	1980W (51.36kJ/cycle)
Coupling Loss	56000W	50670W
Loss of Joints	1890W	1738W
Total Power Loss in CSM	67215W	60803W

Table 7-3.: Average Power Loss of CS Model Coil

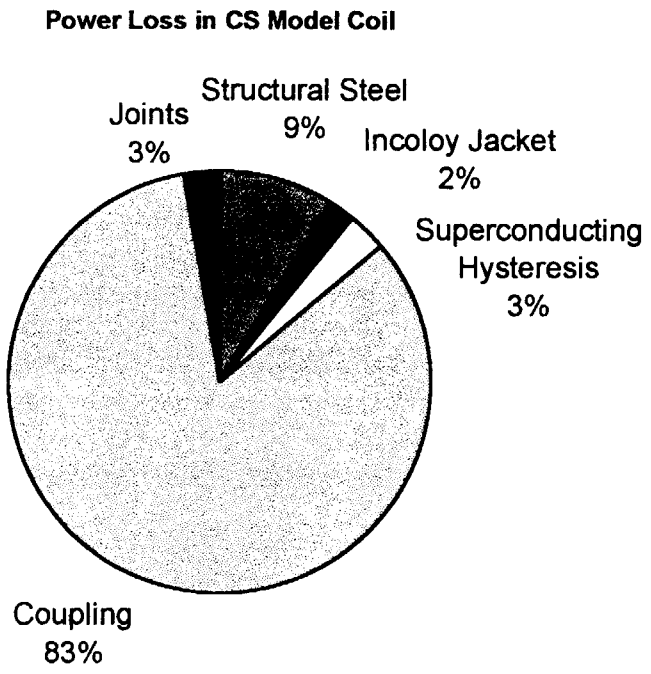

7.6 Time History of Power Loss (without Insert Coil)

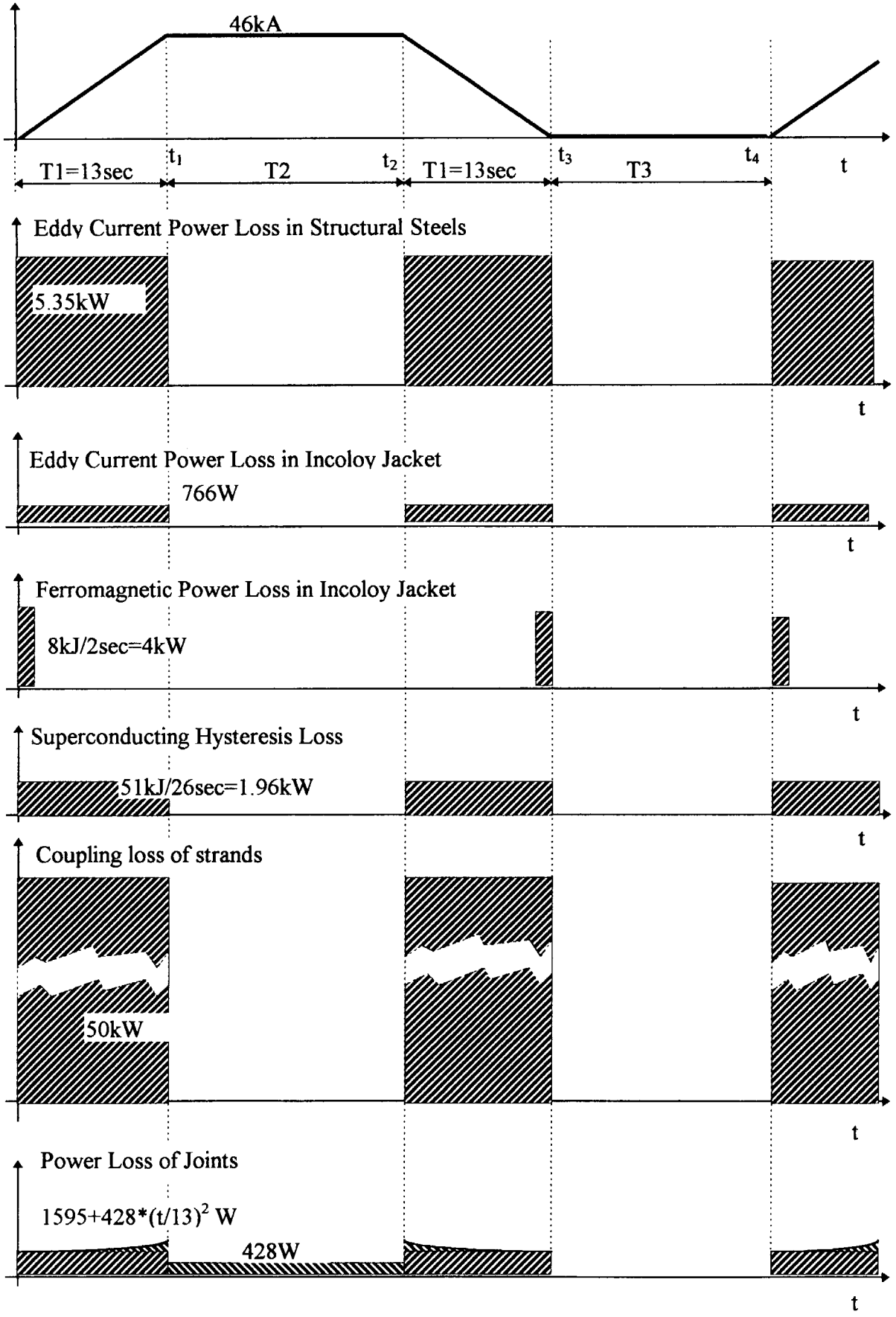

7.7 Decreasing the Loss

Both the eddy current loss and the coupling loss is proportional to the square of flux change rate. They can be drastically decreased if smaller current rate is applied (by increasing the ramp up time). Examples are given in Table 7-4 and Table 7-5.

The eddy current loss can be also decreased if materials having higher specific resistivity values are used. If we allow a temperature increase in structural steels this leads also to the increase of the specific resistivity and hence energy loss decrease. However the most effective method is to change the geometry, cut large size metal components into smaller pieces.

The coupling loss can be decreased by increasing the cross-over resistivity or decreasing the twist-pitch length.

In case of ferromagnetic hysteresis by careful heat treatment the area of BH-curve usually can be decreased or we have to select other material. An other possibility is not to decrease the excitation current back to zero, but keep it on a small level (about 2kA) if the power supply system allow it.

Even if we do not decrease the loss, the energy balance should be kept. This can be done by the proper selection of the T_2 and T_3 time constants which determine the duration of the flat part of the trapezoidal excitation. The cooling system is supposed to operate with constant capacity.

Table 7-4.: Power loss at decreased current rate (equivalent 0.5T/sec)

46kA/26sec (n=0.5)	With Insert Coil	Without Insert Coil
Eddy Current Power Loss of Structural Steel Components	1515W	1337W
Eddy Current Loss of Incoloy Jacket	217W	192W
Ferromagnetic Hysteresis Loss of Incoloy Jacket	154W (8kJ/cycle)	154W (8kJ/cycle)
Superconducting Hysteresis Loss	1045W (54.22kJ/cycle)	990W (51.36kJ/cycle)
Coupling Loss	14000W	12668W
Loss of Joints	510W	470W
Total Power Loss in CSM	17441W	15811W

Table 7-5.: Power loss at decreased current rate (equivalent 0.4T/sec)

46kA/32.5sec (n=0.4)	With Insert Coil	Without Insert Coil
Eddy Current Power Loss of Structural Steel Components	970W	856W
Eddy Current Loss of Incoloy Jacket	139W	123W
Ferromagnetic Hysteresis Loss of Incoloy Jacket	123W (8kJ/cycle)	123W (8kJ/cycle)
Superconducting Hysteresis Loss	836W (54.22kJ/cycle)	792W (51.36kJ/cycle)
Coupling Loss	8960W	8107W
Loss of Joints	338W	312W
Total Power Loss in CSM	11366W	10313W

8. Conclusion

Comparing the AC loss components generated during the energizing process of CS Model Coil, the coupling loss was found to be the largest 83% of the total AC loss supposing 50 msec characteristic time constant. Its main part is generated in Inner Modules.

Also significant amount of heat is generated in structural steels, 9% of the total AC loss. The largest contributions come from lower tension plates and inner tension rods, 58% and 16% of the loss produced in structural steels, respectively. Present calculation shows that cooling is required for stainless steel structural components to avoid the production of hot spots during a longer operation.

Joints should receive special care even if their contribution to the total loss is not so high, because losses are concentrated in a very small volume. An insufficient cooling may cause the quench of the whole magnet starting from joints. Problems may appear with Lap-type joints because of the large AC loss.

The eddy current loss of Incoloy jackets is not significant with the supposed specific resistivity value, 5E-7Ωm. However the real low temperature specific resistivity value should be determined from eddy current measurements and the eddy current loss has to be recalculated. Ferromagnetic hysteresis loss is also produced in Incoloy jackets at the very beginning and at the end of an excitation cycle.

The eddy current and coupling power losses are proportional to the square of flux change rate, so they can be significantly decreased by decreasing the flux change rate. At decreased flux change rate hysteresis losses (superconducting and ferromagnetic) get importance, since the energy loss does not change during a complete cycle. No AC losses are produced following the energizing process of the magnet, when it is driven by a constant excitation current. However Joule losses are produced on the nonzero resistivity of joints by the large transport current. This propose us to keep short the full power operation and increase the time of field free state.

Acknowledgment

The authors would like to thank to Dr. Ohta, general director of Naka Fusion Establishment to make this study possible and also for his kind encouragement. The authors are also thankful to A. Prof. Y. Yoshida and Prof. K. Miya, University of Tokyo for their advice on literature and for their encouragement.

References

[1] K. Simonyi; Theoretical Electricity, Tankonyvkiado, Budapest, 1978.
[2] Wilson; Superconducting Magnet, Clorendon Press, Oxford, 1983.
[3] K. Matsui, Y. Takahashi, M. Nishi, K. Nunoya, T. Kato, H. Nakajima, T. Hiyama, M. Sugimoto, T. Isono, K. Kawano, N. Koizumi, K. Hamada, T. Ando, H. Tsuji, S. Shimamoto, N. Shiga, N. Aoki, M. Ichihara; Design and Fabrication of Superconducting Cables for ITER Central Solenoid Model Coil, IEEE Trans. Magnetics, Vol. 32. No. 4, pp.2304-2307, 1996.
[4] K. Matsui, T. Ito, Y. Takahashi, Y. Nunoya, M. Sugimoto, H. Fujisaki, H. Tsuji, S. Shimamoto; AC Loss Measurement of 46kA Conductor Joint for CS Model Coil, under publication
[5] Ansys Users's Manual for Revision 5.1, SAS IP Inc., 1994
[6] O. Biro, K. Preis; On the use of magnetic vector potential in the finite element analysis of three-dimensional eddy currents, IEEE Trans. Magnetics, Vol 25, No. 4, pp.3145-3159, 1989.
[7] A. Konrad; Integrodifferential finite element formulation of two-dimensional steady-state skin effect problems, IEEE Trans. Magnetics, Vol. 18, No. 1, 1982.

This is a blank page.

国際単位系 (SI) と換算表

表 1　SI 基本単位および補助単位

量	名称	記号
長さ	メートル	m
質量	キログラム	kg
時間	秒	s
電流	アンペア	A
熱力学温度	ケルビン	K
物質量	モル	mol
光度	カンデラ	cd
平面角	ラジアン	rad
立体角	ステラジアン	sr

表 2　SI と併用される単位

名称	記号
分，時，日	min，h，d
度，分，秒	°，′，″
リットル	l，L
トン	t
電子ボルト	eV
原子質量単位	u

1 eV = 1.60218 × 10^{-19} J

1 u = 1.66054 × 10^{-27} kg

表 5　SI 接頭語

倍数	接頭語	記号
10^{18}	エクサ	E
10^{15}	ペタ	P
10^{12}	テラ	T
10^{9}	ギガ	G
10^{6}	メガ	M
10^{3}	キロ	k
10^{2}	ヘクト	h
10^{1}	デカ	da
10^{-1}	デシ	d
10^{-2}	センチ	c
10^{-3}	ミリ	m
10^{-6}	マイクロ	μ
10^{-9}	ナノ	n
10^{-12}	ピコ	p
10^{-15}	フェムト	f
10^{-18}	アト	a

表 3　固有の名称をもつ SI 組立単位

量	名称	記号	他の SI 単位による表現
周波数	ヘルツ	Hz	s^{-1}
力	ニュートン	N	m·kg/s^2
圧力，応力	パスカル	Pa	N/m^2
エネルギー，仕事，熱量	ジュール	J	N·m
工率，放射束	ワット	W	J/s
電気量，電荷	クーロン	C	A·s
電位，電圧，起電力	ボルト	V	W/A
静電容量	ファラド	F	C/V
電気抵抗	オーム	Ω	V/A
コンダクタンス	ジーメンス	S	A/V
磁束	ウェーバ	Wb	V·s
磁束密度	テスラ	T	Wb/m^2
インダクタンス	ヘンリー	H	Wb/A
セルシウス温度	セルシウス度	℃	
光束	ルーメン	lm	cd·sr
照度	ルクス	lx	lm/m^2
放射能	ベクレル	Bq	s^{-1}
吸収線量	グレイ	Gy	J/kg
線量当量	シーベルト	Sv	J/kg

表 4　SI と共に暫定的に維持される単位

名称	記号
オングストローム	Å
バーン	b
バール	bar
ガル	Gal
キュリー	Ci
レントゲン	R
ラド	rad
レム	rem

1 Å = 0.1 nm = 10^{-10} m

1 b = 100 fm^2 = 10^{-28} m^2

1 bar = 0.1 MPa = 10^5 Pa

1 Gal = 1 cm/s^2 = 10^{-2} m/s^2

1 Ci = 3.7 × 10^{10} Bq

1 R = 2.58 × 10^{-4} C/kg

1 rad = 1 cGy = 10^{-2} Gy

1 rem = 1 cSv = 10^{-2} Sv

（注）

1. 表 1 — 5 は「国際単位系」第 5 版，国際度量衡局 1985 年刊行による。ただし，1 eV および 1 u の値は CODATA の 1986 年推奨値によった。
2. 表 4 には海里，ノット，アール，ヘクタールも含まれているが日常の単位なのでここでは省略した。
3. bar は，JIS では流体の圧力を表わす場合に限り表 2 のカテゴリーに分類されている。
4. EC 閣僚理事会指令では bar，barn および「血圧の単位」mmHg を表 2 のカテゴリーに入れている。

換　算　表

力	N(=10^5 dyn)	kgf	lbf
	1	0.101972	0.224809
	9.80665	1	2.20462
	4.44822	0.453592	1

粘　度　1 Pa·s(N·s/m^2) = 10 P(ポアズ)(g/(cm·s))

動粘度　1 m^2/s = 10^4 St(ストークス)(cm^2/s)

圧力	MPa(=10 bar)	kgf/cm^2	atm	mmHg(Torr)	lbf/in^2(psi)
	1	10.1972	9.86923	7.50062 × 10^3	145.038
	0.0980665	1	0.967841	735.559	14.2233
	0.101325	1.03323	1	760	14.6959
	1.33322 × 10^{-4}	1.35951 × 10^{-3}	1.31579 × 10^{-3}	1	1.93368 × 10^{-2}
	6.89476 × 10^{-3}	7.03070 × 10^{-2}	6.80460 × 10^{-2}	51.7149	1

エネルギー・仕事・熱量	J(=10^7 erg)	kgf·m	kW·h	cal(計量法)	Btu	ft·lbf	eV
	1	0.101972	2.77778 × 10^{-7}	0.238889	9.47813 × 10^{-4}	0.737562	6.24150 × 10^{18}
	9.80665	1	2.72407 × 10^{-6}	2.34270	9.29487 × 10^{-3}	7.23301	6.12082 × 10^{19}
	3.6 × 10^6	3.67098 × 10^5	1	8.59999 × 10^5	3412.13	2.65522 × 10^6	2.24694 × 10^{25}
	4.18605	0.426858	1.16279 × 10^{-6}	1	3.96759 × 10^{-3}	3.08747	2.61272 × 10^{19}
	1055.06	107.586	2.93072 × 10^{-4}	252.042	1	778.172	6.58515 × 10^{21}
	1.35582	0.138255	3.76616 × 10^{-7}	0.323890	1.28506 × 10^{-3}	1	8.46233 × 10^{18}
	1.60218 × 10^{-19}	1.63377 × 10^{-20}	4.45050 × 10^{-26}	3.82743 × 10^{-20}	1.51857 × 10^{-22}	1.18171 × 10^{-19}	1

1 cal = 4.18605 J（計量法）

= 4.184 J　（熱化学）

= 4.1855 J　（15 °C）

= 4.1868 J（国際蒸気表）

仕事率　1 PS（仏馬力）

= 75 kgf·m/s

= 735.499 W

放射能	Bq	Ci
	1	2.70270 × 10^{-11}
	3.7 × 10^{10}	1

吸収線量	Gy	rad
	1	100
	0.01	1

照射線量	C/kg	R
	1	3876
	2.58 × 10^{-4}	1

線量当量	Sv	rem
	1	100
	0.01	1

（86 年 12 月 26 日現在）

AC LOSS CALCULATION OF CENTRAL SOLENOID MODEL COIL